# Performance augmentation and machine learing-based modeling of wavy corrugated solar air collector embedded with thermal energy storage: Support vector machine combined with Monte Carlo simulation

Mohamad E. Zayed[a*], A. E. Kabeel[b,c], Bashar Shboul[d], Waqar Muhammad Ashraf[e], Mohamed Ghazy[f], Kashif Irshad[a], Shafiqur Rehman[a], Abdelhameed A. A. Zayed[g]

[a]Interdisciplinary Research Center for Renewable Energy and Power Systems, King Fahd University of Petroleum and Minerals, Dhahran 31261, Saudi Arabia.
[b]Mechanical Power Engineering Department, Faculty of Engineering, Tanta University, Tanta 31521, Egypt.
[c]Delta University for Science and Technology, Faculty of Engineering, Gamasa, Egypt.
[d]Department of Renewable Energy Engineering, Faculty of Engineering, Al Al-Bayt University, Mafraq, Jordan.
[e]The Sargent Centre for Process Systems Engineering, Department of Chemical Engineering, University College London, Torrington Place, London WC1E 7JE, UK.
[f]Department of Mechanical, Faculty of Technology and Education, Sohag University, Sohag, 82524, Egypt.
[g]Production Engineering and Mechanical Design Department, Faculty of Engineering, Tanta University, Tanta, Egypt.

***Corresponding author**: Mohamed E. Zayed

**E-mail address**: Mohamed.zayed@kfupm.edu.sa

**ORCID**: https://orcid.org/0000-0002-8641-8584

## Abstract

At present, artificial intelligence methods have been effectively utilized for predicting the complex performance of storage-based solar thermal technologies for cooling/heating applications. It is crucial to have accurate energy storage-based sustainable system estimation, which would contribute to increased operational time, thus maximizing the overall efficiency of solar energy-based storage systems. Hence, this work introduces a comparative experimental investigation and support vector machine (SVM) modeling on a wavy corrugated solar air collector (WCSAC) with and without using a paraffin wax storage container. Experiments on the WCSAC were performed under three air flow rates of 0.540, 1.68, and 3.72 kg/min and two paraffin layer thicknesses of 2 cm and 4 cm, respectively. Moreover, improved SVM models implemented in MATLAB software are developed for predicting the thermal performance parameters; including air temperature ratio, average air temperature, convective heat transfer coefficient, and energy efficiency for the WCSAC. The optimal solution of the SVM modeling is developed by incorporating the Karush-Kuhn-Tucker conditions and several kernel functions. In addition, a sensitivity analysis is also conducted to explore the significance of model input parameters (air inlet temperature, time, solar irradiance, air flowrate, PCM layer thickness) on the output parameters prediction using the Monte

Carlo simulation technique. The experimental results presented that the daily energy efficiencies of the WCSAC equipped with 4 cm paraffin layer thickness are 24.0%, 20.39%, and 16.37% higher than that of the WCSAC without PCM at airflow rates of 3.72, 1.68, and 0.54 kg/min, respectively. Moreover, the connective heat transfer coefficient of the WCSAC with PCM is more than 1.20 times that yielded with the WCSAC without PCM. Additionally, the SVM simulations showed that the optimal solution of the SVM model is developed by incorporating the Karush-Kuhn-Tucker conditions and Lagrangian function kernel function, which revealed a superior with the highest coefficient of determination of 0.990 and 0.950 for training and test processes, respectively.

**Keywords:** Solar air collector; Wavy corrugated absorber; Phase change materials; Support vector machine modeling; Monte Carlo simulation; Energetic and exergetic performance analysis.

**Nomenclature**

| **Abbreviations** | | | |
|---|---|---|---|
| ANN | Artificial Neural Network | $M_a$ | Air flowrate, kg/s |
| CHTC | Convective Heat Transfer Coefficient | $T_{amb}$ | Weather temperature, K |
| PCM | Phase change materials | $T_a$ | Mean air temperature, K |
| SVM | Support Vector Machine | $T_p$ | Mean absorbent temperature, K |
| WCSAC | Wavy Corrugated Solar Air Collector | $T_s$ | Temperature of the sun, K |
| **Symbols** | | $T_{out}$ | Exit air temperature, K |
| $A_{ab}$ | Projected area of Absorber, $m^2$ | $t_{ins}$ | Insulation thickness, mm |
| $C_p$ | Air heat capacity, (J/kg K) | U | Uncertainties in the output |
| $E_{x,\,des}$ | SAC exergy destruction, W | **Greek symbols** | |
| $E_{x,\,in}$ | SAC input exergy, W | L (α) | Loss function of the SVM |
| h | Heat transfer coefficient by convection, $W/m^2.K$ | $\alpha_n$ | Non-negative number |
| $y_i$ | Corresponding output variable | ΔT | Air temperature difference, K |
| I | Solar irradiation, $W/m^2$ | $\xi$ | Slack index |
| K | Thermal conductivity, W/m.K | η | Efficiency, % |
| $K(.)$ | Kernel function | ε | Emissivity, % |

## 1. Introduction

The development of new, cost-effective energy supplies has taken precedence due to the significantly increased global energy demand in order to address these difficulties [1, 2]. International Energy Agency has indicated that energy consumption in the globe will increase by about 50% from 2018 to 2050 [3]. With this energy consumption trend, the world's fossil fuels will run out by 2042 [4]. Numerous alternative sources that can generate eco-friendly energy at a low cost are known as sustainable energy resources [5, 6]. Among these resources, solar energy is an environmentally friendly energy source that can be considered for supplying electrical and thermal energies [7, 8]. By way of the convertibility of solar energy into heat, solar air collectors (SACs), as a sustainable solar technology, aim at delivering heated and fresh air for drying medical and agricultural products [9, 10]. The SAC consists of a test section in between the divergent and convergent ducts which are the inlet and outlet of the SAC, respectively. The primary principle behind SAC is forcing to provide enough quantity of air through the duct to primarily remove the heat that has been accumulated in the absorber plate [11]. In light of achieving high efficiency of heat transfer between the absorptive surface and air, the preferable and widely used method for pushing air through the SAC is the forced convection method, which is achieved better heat transfer performances than the natural air convection mode [12]. Simple design, flexibility, cleanness, compactness, and easy maintenance are considered the main advantages of SACs besides their utility in numerous applications, specifically space heating and product drying utilities [13, 14].

The combinations of storage materials either latent storage materials (paraffins, palmitic acid, hydrate salts) or sensible storage materials (gravel, granite, sand, phosphate pellets, porous sponges) in solar air collectors under the absorber plate represents the up-to-date progress in SAC designs which simplifies the design keeping compactness and low-cost storage beds when compared to separate storage units [15]. Amongst them, phase-change materials (PCM) as a commonly latent energy storage medium, are used in solar air/water heating applications because of their relatively stable solidification/ melting temperature and high energy density [16]. Moreover, energy storage materials have been shown to improve the generated freshwater and reduce the specific energy consumption and freshwater unit cost of solar desalination systems [17, 18]. An experimental study was done by Kabeel et al. [12] to compare the performance of the SAC employing corrugated and flat absorbent plates embedded with paraffin wax as PCM as the TES material. The results showed the superiority of the SAC with a V-corrugated plate over the

flat plate with 15% higher thermal behavior. A temperature of 1.5–7.2 °C of the exit air was achieved 3.5 hours after nightfall. In another experimental research, an increase of 4 to 16°C in the hot exit temperature of the air over the ambient temperature was recorded during the whole night by Khardraui et al. [19] by utilizing a SAC of length 2.04 m and width of 1.04 m, and a container with a rectangular shape to enclose a PCM unit of thickness 0.05 m. More so, some attempts are also being made by researchers to have economically and environmentally effective solar dryers based on SACs for dyrying crops.. An indirect solar dryer integrated with a thermal storage system with PCM was used for medicinal herb drying by Bhardwaj et al. [20]. Paraffin RT-42 was used for thermal storage which reduced the drying time of the herb by 37.5% and 64.29% as compared with heat pump drying and shade drying, respectively. Azaizia et al. [21] carried out an experimental analysis of a mixed type greenhouse dryer with the thermal storage system and analysed the effect of using paraffin wax as the thermal storage material on the drying efficiency with red pepper.

On the other hand, increasing the surface area of the absorber results in more effective SACs. One way to achieve this is to use the v-corrugated plate. Three SACs were designed and examined for comparison in an experimental study conducted by Das et al. [22]. The three absorbent configurations were jet-to-corrugated, cross-flow corrugated, and jet-to-flat absorber plates. The results revealed that the most efficient type in terms of maximum thermal effectiveness was the jet-to-flat plate type yielding fewer temperature fluctuations between the absorber and the outlet air temperature. The effect of using heat exchangers and water-air reflectors on the overall efficiency of the SAC employing a v-corrugated absorber was analysed by Shallal and Eleiwi [23]. It was reported that by using the reflectors, the maximum daily efficiency increased from 59.95 % to 63.49 %. Three types of SACs were designed and manufactured by Tuncer et al [24]. The three types under consideration were double-pass, parallel-pass as well as v-groove SACs. The results of comparisons among the three SACs showed that the maximum mean thermal efficiencies were 78.2%, 67%, and 60.3% for double-pass, parallel-pass, and v-groove SACs, respectively.

Additionally, a few numerical investigations on the design of SACs with integrated PCM have been also presented, along with the impact of various geometrical and operational parameters as well as the performance-improving strategies including the type of airflow and heat-exchanging surfaces. Using Ansys, Raj et al. [25] investigated numerically a SAC embedded with a micro-

encapsulated PCM. Based on the melting and solidification results, it was recorded that for using a cylindrical container of 0.1 m and 0.07 m for length and diameter, respectively, a great portion, 70%, of the PCM was totally melted. The influences of air flowrate, stream pitch distance, and jet diameter were theoretically investigated and optimized showcasing their influence on the behavior of SAC in the study done by Matheswaran et al. [26]. Nagale et al. [27] carried out a numerical analysis on recyclic SAC employing an integrated wavy corrugated TES system. A noticeable rise in the temperature of outlet air of 9 °C as compared to the ambient was reported based on the results. Kumar et al. [28] introduced a SAC with the absorber plate having a V-corrugated shape and the shot-blasting method was used to modify the inner surface. It was indicated that the efficiencies of the average energy of the proposed SAC related to different values of air flowrate of 0.01, 0.015, and 0.02 kg/s, as compared to the traditional SAC were increased by around 2.4%, 3.1%, and 5.8%, respectively. In the numerical study of Kashyap et al. [29], the influence of roughness parameters on the behavior of SAC utilizing different v-rib patterns with multiple symmetrical gaps rib elements was investigated. It was reported that the roughness had a significant effect as the Nusselt number and pressure drop, which were increased by 6.50 and 5.70 times that of the traditional smooth SAC, respectively.

In spite of numerical approaches showing well-established methods for forecasting a SAC's thermal behavior, however, numerical models have a significant computing cost and need to be rigorously validated and verified using experimental research. To overcome these limitations of high computing time and expensive cost, artificial intelligence methods, such as artificial neural networks (ANN), have been considered to forecast the SAC's thermal performance. Nidhul et al [30] forecasted the thermal behavior of ribbed triangular duct SAC using a traditional ANN model. The predictive fractional coefficient and Nusselt number were forecasted by the proposed ANN model achieving an average deviation of less than 3%. Another ANN model was proposed by Aidinlou and Nikbakht [31] to depict the thermohydraulic requirements of constant geometrical parameters of SACs. The ANN model was feasible for predicting the fluid flow and heat transfer of the SAC. A multiple linear regression network (MLRN) approach was compared to the ANN model by Shettey et al. [32] to predict the thermohydraulic behavior of a circular-perforative absorbent plate SAC. The outputs displayed that the ANN surpassed the MLRN model. Moreover, the ANN model was compared to wavelet neural network (WNN) models proposed by Esen et al. [33] to study the performance of SAC, and the WNN showed higher accuracy than ANN.

Furthermore, another comparison among three models, namely, adaptive network-based fuzzy inference system (ANFIS), grey modelling (GM), and ANN was held by Erenturak and Erenturak [34] to investigate a SAC's thermal performance. According to the results, accurate prediction of the output air temperature was simply gained by GM easier than the other two models. Also, Saravanan et al. [35] developed three models; namely, K-nearest neighbors (KNN), random forest (RF), and linear regression network (LRN) forecasting models were compared to predict a C-shaped SAC's thermal behavior utilizing three dependent output variables; namely, thermal efficiency, Nusselt number, and frictional factor . It was revealed that the RF model outweighed the LRN and KNN models.

It is clear from the aforementioned ANN research that diverse SAC designs have not been fully taken into account when predicting performance under a variety of circumstances. The majority of earlier models used traditional ANN techniques, which only took into account the connection between the output and hidden layers and ignored the connectivity between the output and input layers. Considering the prior outcomes, it is clear that this could result in an overfitting issue and lower the method's prediction accuracy. To address these limitations, effective machine learning models such as support vector machines (SVM) are employed to solve complicated issues [36]. The SVM model features a thorough Bayesian framework used to obtain scattering solutions for regression (estimator) and classification tasks using nonlinear relationships between parameters [37]. The advantage of the Bayesian method is that it can be smoothly performed in the SVM framework, resulting in subsequent computational acceleration from a practical point of view [38]. The assumed large margin and the kernel role make the SVM perform better than ANN. Additionally, diversified parameters such as the number of hidden layers and their hidden neurons, number of iterations, learning rate, and momentum factor are acquired to be selected carefully for the ANN.

So far, scholars are still seeking the development of newly configurations that can increase the overall performance of the SACs. Moreover, the above-summarized review indicates that there are no previous studies have been focused on modeling the performance of the SACs using support vector machine (SVM) models. Subsequently, the current work attempts to fill this gap by figuring out the applicability of SVM models to fulfill a non-linear relationship between performance outputs and the effectual performance input parameters of SACs. Therefore, there are two main

contributions to this study. The first contribution is conducting a comparative experimental study on the dynamic thermal performance of a wavy corrugated solar air collector (WCSAC) with and without using paraffin wax, which is simultaneously constructed and tested under climatic conditions of Tanta, Egypt, for three air flow rates of 0.54, 1.68 and 3.72 kg/min. The second contribution is applying different SVM models to predict the performance parameters (air temperature ratio, average air temperature, convective heat transfer coefficient, and energy efficiency) of the WCSAC with and without the usage of PCM. The SVM models are trained using the obtained experimental data of the WCSAC and are evaluated using two different statistical measures. The third contribution is to investigate the complete design space of the input variables and thus, the impact of each input variable on each output variable. Wherefore, a comprehensive approach to assess the significance of model input parameters in SVM models using the Monte Carlo simulation technique.

The intrinsic novelties of this research are:

1. Assessment of the experimental performance of the PCM-storage-based WCSAC and comparing it with that of a WCSAC without PCM in terms of heat transfer behavior, as well as energetic and exergetic aspects.
2. Developing improved SVM models for predicting the thermal performance parameters of the two cases of investigated SACs. The optimal solution to the non-linear dual problem in SVM is developed by incorporating the Karush-Kuhn-Tucker conditions and several kernel functions.
3. Evaluating the significance of model input parameters (air inlet temperature, time, solar irradiance, air flowrate, PCM layer thickness) in SVM models for prediction of the output parameters of the WCSAC using the Monte Carlo simulation technique.

This manuscript is arranged as follows. The experimental system of the proposed WCSAC is illustrated in Section 2. The modeling approach, structure steps, and assessment criteria for SVM-based estimation algorithms and Monte Carlo simulation are explained in Section 3. Both comparative experimental analysis and prediction simulation results are demonstrated in Section 4. Lastly, most of the important conclusions have been outlined in Section 5.

## 2. Experimental apparatus

### 2.1. Design and construction

Figure 1 exhibits the 3-D drawing of the experimental test rig of the proposed WCSAC system. The main parts of this apparatus are the SAC with the wavy corrugated absorbent plate having a PCM closed channel below it and a centrifugal blower. To connect these two main parts, a PVC pipe with an inner diameter of 10.5 cm is utilized while the air flow rate is controlled by a gate valve in-between. ASHRAE recommendations are the guide for designing and manufacturing the WCSAC, which have been applied using obtainable domestic materials [39]. A 1 mm thick copper sheet is used as the material for the corrugated plate. The corrugation formed with a V-shape with a corrugation angle of $60^{o}$ and a v-groove height of 21.5 mm, respectively. This produces a projected area of solar intensity of 1.0 $m^2$ with an effective heat transfer area equal to 2 $m^2$. So as to increase the solar absorption rates, the absorbent plate was painted with mat black paint. Moreover, to decrease the thermal losses from the surface of the absorber plate, a 4 mm thick glass sheet was utilized keeping a 5 cm space between the plate and the glass sheet. PCM container with 4 cm depth and 1×1 $m^2$ area was used as PCM bed, which is located under the absorber plate. Paraffin wax was utilized as PCM due to its several merits such as chemical stability, low cost, high-density storage, and availability in Egypt [40], which are the causes to use this PCM type as energy storage material. The thermophysical features of the utilized paraffin wax are introduced in Table 1. Molten paraffin wax amounts of 38 and 19 kilograms corresponding to PCM layer thicknesses of 4.0 and 2.0 cm as the PCM was used and examined to totally fill the closed channel. Molten paraffin wax was poured through an external port on the side of the SAC so that the paraffin surface was completely in contact with the absorber surface. To guarantee that the paraffin is perfectly in contact with the absorber surface, an outside channel on the side of the heater was used as the location of pouring the paraffin. A foam layer of thickness 5 cm was used to insulate the bottom of the closed channel and heater's sides. To avoid the air downstream effect at the outlet of the heater, a conic rectangular exit section was attached to the SAC outlet pipe 20 cm in length. Furthermore, to prevent any leakage of the PCM, the WCSAC was installed in a horizontal way as displayed in Fig. 1.

Table 1. Characteristics of the utilized paraffin wax.

| No. | Property | value |
|---|---|---|
| 1 | Fusion temperature | 54 $^{o}$C |
| 2 | Fusion latent heat | 190 kJ/kg.$^{o}$C |

| | | |
|---|---|---|
| 3 | Thermal conductivity | 0.21 W/m.$^{o}$C |
| 4 | Solidified density | 877 kg/m$^{3}$ |
| 5 | Liquified density | 796 kg/m$^{3}$ |
| 6 | Specific capacity | 2.13 kJ/kg.$^{o}$C |

**(a)**

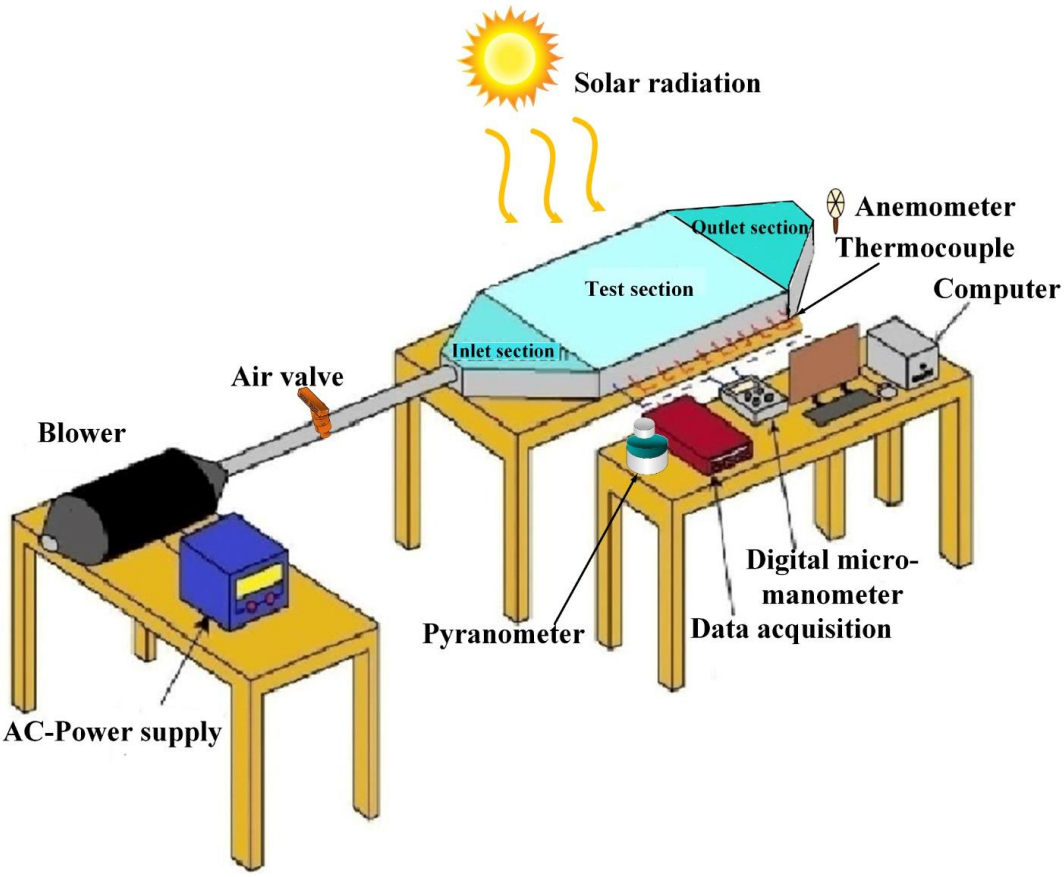


**(b)**

**(c)**

Fig. 1. Schematic diagram of the experimental setup, (b) Photographic viewfor the experimental system of wavy corrugated SAC, and (c) Pictorial view of the utilized wavy curragted absorber configeration.

### 2.2. Measurement and experimentation procedures

The present study on the wavy corrugated solar air collector (WCSAC) was implemented experimentally in Tanta city (30° 43′N, 31°E), Egypt, with and without using paraffin wax, for three air flow rates of 0.54, 1.68, and 3.72 kg/min. The duration of the experiments was from 8:00 a.m. till mid-day at 12 p.m. Also, there was no considerable variation in the meteorological conditions, because of the stable, sunny, and clear weather for successive days. The inlet, outlet, and ambient air temperatures besides the solar radiation and the velocity of airflow represent the factors to be measured. The solar intensity was recorded using a pyranometer (MS-802 model), while the airflow velocity was measured by a Testo 405-V1 anemometer having a range of 0.2–10 m/s and accuracy ±0.2 m/s. For the sake of simultaneously and automatically collecting accurate readings of different temperatures and solar radiation from digital temperature sensors and a pyranometer every five minutes, respectively. These sensors were connected to an ARDUINO board which in turn was connected to a Laptop to import recorded data to Excel and save these data for post-processing. For blowing air through the SAC, a fan of 0.4 m diameter was driven by a three-phase induction motor with the power of 3 horsepower and a maximum revolution per minute of 2810 r/min and input electrical parameters as 3.5 A, 390 V, and 50 Hz.

### 2.3.Uncertainty analysis

Experimental data are recorded throughout the experimental run using appropriate measurement devices. However, uncertainties may arise due to errors in gauges, sensor locations, indicator readings, and ambient conditions. Estimating the uncertainty of experimental results for various parameters is therefore essential to highlight the errors that appear in experimental results. Table 2 shows the measuring range and accuracy of each of the measuring equipment used in this work.

**Table 2.** Accuracies of the measuremental tools involved in the conducted experimentations.

| Measuremental device | Range | Accuracy |
|---|---|---|
| Temperature sensors | 0 – 300 °C | ± 0.20 % |
| Solar powermeter | 0 − 2000 W/m$^2$ | ± 5.0 % |
| U-tube manometer | 0 – 50 mm | ± 5.0 % |

| | | |
|---|---|---|
| Anemometer | 0 – 30 m/s | ± 0.20 % |
| Data logger | – | ± 0.01 % |

Holman approach [41] introduced before for uncertainty analysis will be followed in this study. Consider that the output Z is a function of the independent variables $Y_1$, $Y_2$, $Y_3$, ..., $Y_n$.

$$Z = f(Y_1, Y_2, Y_3, ..., Y_n) \quad (1)$$

Let $U_z$, $U_1$, $U_2$, $U_3$…, and $U_n$ be the uncertainties in the output and the independent variables $Y_1$, $Y_2$, $Y_3$, ..., $Y_n$, respectively. $U_z$ can be calculated as follows [41];

$$U_Z = [(U_1\,\partial Z/\partial Y_1)^2 + (U_2\,\partial Z/\partial Y_2)^2 + \cdots + (U_n\,\partial Z/\partial Y_n)^2]^{0.5} \quad (2)$$

Table 3 presents the experimental uncertainties introduced during the experimental tests in measuring various thermal parameters of WCSAC.

**Table 3.** Uncertainty computations of diversified operational parameters of the WCSAC.

| **Item** | Uncertainty ($U_Z$) |
|---|---|
| Solar irradiation | ± 1.41 % |
| Air flowrate | ± 0.87 % |
| Air temperature | ± 0.17 % |
| Air pressure drop | ± 0.35 % |
| **Overall uncertainty** | ± 1.70 % |

### 2.4 Performance analysis modeling

This section presents the formulation of the equations that govern and describe the energetic, thermo-hydraulic, and exergetic performance of the WCSAC.

#### 2.4.1 Energy analysis

The WCSAC's beneficial heat gain can be expressed as [12];

$$Q_u = \int_0^t m_a\, C_{p,a}\, dT \quad (3)$$

Here, $m_a$ (kg/s), $C_{pa}$ (J/kg K), are the air mass flow rate and specific heat capacity, respectively. The differential in the difference between outlet and inlet air temperatures is denoted by $dT$ (K).

Mathematically, the overall absorbed heat by the surface of the absorber is represented as [42];

$$Q_{absorbed} = \left( \int_0^t I(t) \times \tau_g \times \tau_a \times \alpha_{ab} \times A_{ab} dt \right) - U_b A_{ab} \left( T_b - T_a \right) \quad (4)$$

Here, *I (t)* is the totally solar intensity in W/m$^2$, $A_{ab}$ is the projected cross-sectional area of the absorber in m$^2$, the absorbent plate's absorptivity is denoted by $\alpha_{ab}$, and $\tau_g$ is the glazier cover transmittance. While $T_a$ is the flowing air's average temperature and $T_b$ is the absorbent plate's average temperature.

The mathematical expression for the heat transfer in the convective mode between fluid and the surface of the absorber is expressed as [12];

$$h = \int_o^t \frac{m_a \, C_{p,a} \, dT}{(T_p - T_a)} \quad (5)$$

The WCSAC's average energy daily efficacy is denoted by $\eta_{en}$ is the ratio between the sum of the hourly beneficial heat gain obtained by the air and the daily solar intensity fallen on the absorber's surface projected area. This efficiency is computed as [12];

$$\eta_{en} = \int_0^t \frac{m_a \, C_{p,a} \, dT}{I(t) \, A_{ap}} \quad (6)$$

### 2.4.2 Thermo-hydraulic analysis

In this study, forced convection is employed as the heat transfer way for the proposed WCSAC. Consequently, the the forced air flowing via the collector wavy duct requires pumping power expenses which should be taken into account. Therefore, the thermohydraulic efficiency of the WCSAC, $\eta_H$, is introduced and defined as the difference between the useful heat gain and the pumping power ($Q_u - P_f$), to the total solar input as presented in Eq. (7) [43];

$$\eta_H = \int_0^t \frac{\left[ Q_u - P_f \right]}{I(t) \, A_{ap}} = \int_0^t \frac{\left[ (m_a \, C_{p,a} \, dT) - P_f \right]}{I(t) \, A_{ap}} \quad (7)$$

where the mathematical expression of the pumping power $P_f$ is [43];

$$P_f = \frac{m_a \, \Delta P}{\rho_a} \quad (8)$$

and the decrease in pressure, $\Delta P_s$, through the test section for a smooth flow channel considering no storage of energy is given as [43];

$$\Delta P_s = 2 \, f_s \, L \, \rho_a \, v_a^2 / D_h \quad (9)$$

Where $\rho_a$ denotes the average density of the air having a value of 1.204 g/m$^3$, $L$ represents the WCSAC's length and the continuity formula is employed to calculate the average velocity of the air, $v_a$, as follows;

$$v_a = \frac{m_a}{\rho_a A_{ap}} \quad (10)$$

Based on the values of the perimeter of the heater duct, $P$, and the projected cross-sectional area, $A_{ap}$, the WCSAC duct's hydraulic diameter $D_h$ is calculated as:

$$D_h = \frac{4 A_{ab}}{P} \quad (11)$$

The value of the $f_s$, which is the coefficient of friction for a non-porous flow channel, is based on the type of the flow as follows [43];

$$f_s = \frac{64}{Re} \quad \text{For laminar flow} \quad (12)$$

$$f_s = \frac{0.059}{Re^{0.20}} \quad \text{For turbulent flow} \quad (13)$$

The formula for the Reynolds number, $Re$, is;

$$Re = \frac{\rho_a v_a D_h}{\mu_a} = \frac{m_a D_h}{A_c \mu_a} = \frac{4 m_a}{\pi D_h \mu_a} \quad (14)$$

Additionally, the pressure loss through the WCSAC, $\Delta P_{por}$, is calculated using the quadratic formula introduced by Tien and Vafai [44] as given:

$$\frac{\Delta P_{por}}{L} * \frac{D_h^2}{v_a \mu_a} = \frac{D_h^2}{K} + \frac{\gamma D_h}{\sqrt{K}} Re \quad (15)$$

Where $\mu_a$ represents the dynamic viscosity of air having a value of 1.89*10$^{-5}$ Pa.s, whereas $K$ and $\gamma$ are the permeability and inertial coefficient of the absorbent material.

### 2.4.3 Exergy analysis

The WCSAC exergy efficiency is defined as the ratio of the whole acquired exergy due to the beneficial heat gain rate by the air $E_{x,\,dex}$ to the totality of perpetuity obtainable exergy from the sun fall on the WCSAC, $E_{x,\,in}$ [42]. The efficiency is mathematically expressed as;

$$\eta_{ex} = \int_0^t \frac{E_{x,des}}{E_{x,in}} \quad (16)$$

The WCSAC exergy destruction is given as;

$$E_{x,destruction} = Q_u \left(1 - \frac{T_{out}}{T_a}\right) \quad (17)$$

Also, the WCSAC input exergy is expressed as;

$$E_{x,\text{in}} = \left(1 - \left(\frac{4}{3} \times \frac{T_a}{T_s}\right) + \left(\frac{1}{3} \times \left(\frac{T_a}{T_s}\right)^4\right)\right) \times I(t) \quad (18)$$

where $T_{out}$ refers to the exit air temperature and the sun's temperature, $T_s$ is considered as 5727 $^{o}$C [45].

## 3. Support vector machine-based process models

SVM is one of the powerful modelling algorithms of machine learning and can accurately predict the response values for the complex system that is defined on hyperdimensional input space. Furthermore, the SVM model possesses good generalization potential in predictive analytics [46, 47]. The structural risk minimization principle is employed for the SVM model development. The data is effectively separated by the hyperplane to improve prediction accuracy, while the margin surrounding the hyperplane is expanded to accommodate prediction errors within a specified limit as shown in Fig. 2 (a). Nonlinear SVM is generally used for problems that possess nonlinear and complex characteristics. For this, data is projected into higher dimensions, and the problem is solved in a linear pattern. Different kernel functions like linear, quadratic, cubic, Gaussian, etc., can be used for the development of an SVM model having good prediction performance. It is important to mention here that SVM utilizes Vapnik's ε-intensive loss function and formulates the supposition problem as an optimization problem with inequality constraints, aiming to maximize the margin around the hyperplane [48]. By solving a quadratic programming problem, SVM is capable of capturing the nonlinear relationship among variables. The mathematical expression for the nonlinear SVM model is given as:

$$\{(x_i, y_i), i = 1,2,3, \dots, N\} \qquad x_i \in R^d,\ y_i \in \{R^d\} \quad (19)$$

where, $x_i$ is the vector of input variables and $y_i$ is the corresponding output variable; $i = 1,2,3, \dots, N$ equal to the total number of observations of the training dataset. The loss function for the nonlinear SVM model combined with the Lagrangian function is introduced and can be written as reported in Refs. [46, 47];

$$L(\alpha) = \frac{1}{2}\sum_{i=1}^{N}\sum_{j=1}^{N}(\alpha_i - \alpha_i^*)(\alpha_j - \alpha_j^*)K(x_i, x_j) + \varepsilon\sum_{i=1}^{N}(\alpha_i + \alpha_i^*) + \sum_{i=1}^{N} y_i(\alpha_i - \alpha_i^*) \quad (20)$$

Subject to the constraints as given:

$$\sum_{i=1}^{N}(\alpha_n - \alpha_n^*) = 0 \quad (21)$$

$$\forall n: 0 \leq \alpha_n \leq C \quad (21)$$

$$\forall n: 0 \leq \alpha_n^* \leq C \quad (22)$$

Here, $\alpha_n$ and $\alpha_n^*$ are the non-negative numbers, $K(.)$ represents the kernel function responsible for projecting the input space into higher dimensions; $\varepsilon$ represents the epsilon margin around the hyperplane, and $C$ denotes the penalty parameter. The optima of the non-linear dual problem in SVM is developed by incorporating the Karush-Kuhn-Tucker conditions which are given as:

$$\forall n: \alpha_n^*[\varepsilon + \xi_n + y_n - f(x_n)] = 0 \quad (23)$$

$$\forall n: \alpha_n[\varepsilon + \xi_n - y_n + f(x_n)] = 0 \quad (24)$$

$$\forall n: \xi_n^* (C - \alpha_n^*) = 0 \quad (25)$$

$$\forall n: \xi_n(C - \alpha_n) = 0 \quad (26)$$

Here, $\xi$ and $\xi^*$ symbolize the slack indexes that tolerate the deviations beyond the $\varepsilon$-tube. Finally, the SVM model can be written as:

$$Y(x) = \sum_{i=1}^{N}(\alpha_i + \alpha_i^*)K(x_i, x) + b \quad (27)$$

Here, $Y(x)$ is the output variable that is to be predicted by the set of input variables $(x)$ and $b$ is the bias value. The network structure of the employed SVM model is systematically displayed in Fig. 2 (b).

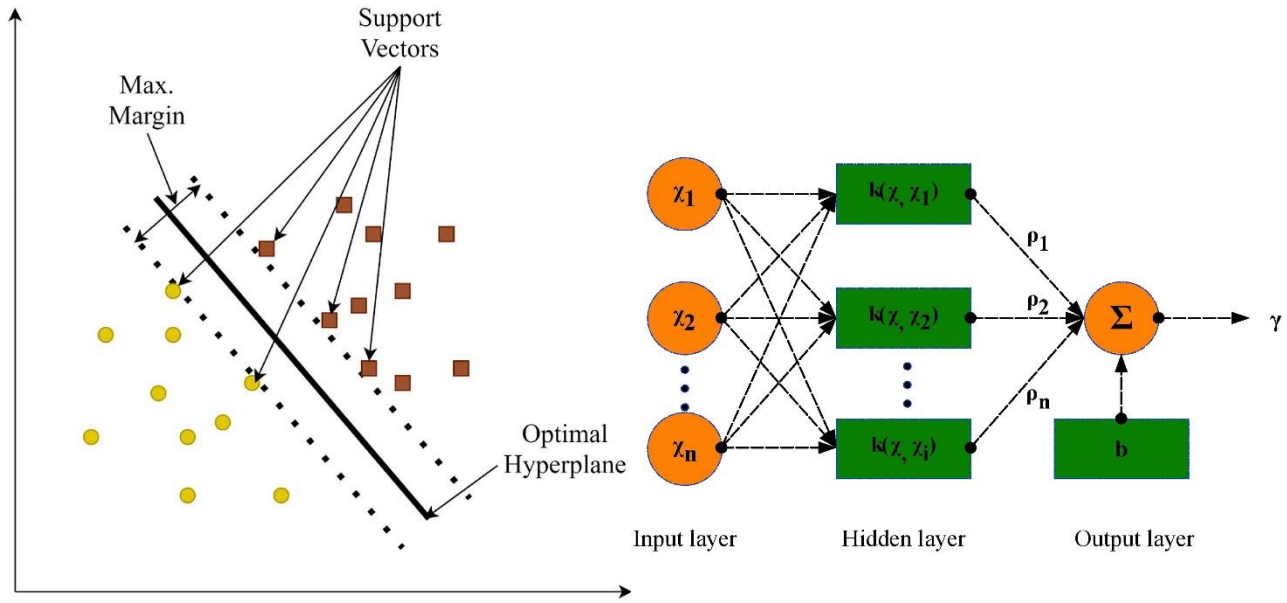


Fig. 2. (a) Hyperplane in a 2-D feature domain; (b) Network structure of SVM.

### 3.1 Evaluation criteria

To assess the modeling accuracy of the developed SVM models, The predictive performance of the SVM models is evaluated on the rigorous statistical measures as introduced in the section; evaluation criteria based on rigorous performance evaluation measures should be employed. In this regard, two statistical measures, namely the determination coefficient ($R^2$) and root mean squared error (RMSE), are utilized [49]. The mathematical expression of $R^2$ and RMSE is given as:

$$R^2 = 1 - \frac{\sum_i^N (y_i - \hat{y}_i)^2}{\sum_i^N (y_i - \bar{y}_i)^2} \tag{28}$$

$$RMSE = \sqrt{\frac{1}{N}\sum_{i=1}^{N} (\hat{y}_i - y_i)^2} \tag{29}$$

here, $y_i$ represents the actual value of the output variable, while $\hat{y}_i$ is the simulated response of the SVM model. Likewise, $\bar{y}_i$ denotes the mean value of $y_i$, and $i$ takes values from 1 to N, representing the total number of observations. The coefficient of determination ($R^2$) serves as a metric for assessing the accuracy of the SVM model's predictions against the actual output values. Its value ranges from 0 (indicating poor predictability) to 1 (indicating a strong functional relationship between the input and output variables). On the other hand, the root-mean-squared

error (RMSE) measures the deviation between the simulated responses of the ML model and the actual output values.

### 3.2 Significance analysis of the input variables on the output variables

The machine learning model constructs the functional mapping between the input-output variables based on the training observations. Having trained an ML model possessing excellent predictive and generalization performance, it is important to establish the relative importance of the input variables towards the predictions of the output variables. The Monte Carlo technique is a comprehensive method that is suitable for this task; a large number of experiments are constructed on the operating ranges of the variables and are simulated by the developed ML model. A large number of simulated experiments allow us to investigate the complete design space of the input variables and thus, the impact of the input variable on the output variable can be studied. Hence, this paper also investigates the complete design space of the input variables and thus, the impact of the input variable on the output variable. Wherefore, a comprehensive approach to assess the significance of model input parameters in SVM models using the Monte Carlo simulation technique.

#### 3.2.1 Monte Carlo simulation technique

Monte Carlo technique is a comprehensive method that is suitable for this study; a large number of experiments are constructed on the operating ranges of the variables and are simulated by the developed ML model. Many simulated experiments allow us to investigate the complete design space of the input variables and thus, identify the influence of each input variable on each output variable.

The Monte Carlo simulation method has been adopted to produce random samples from a provided probability distribution. The adopted technique could be used in parametric significance analysis in order to generate several sets of simulated data. Every sample of the simulated data is implemented to be simulated from the trained SVM model and the impact of the input variable on the output variable is computed. This paper presents a comprehensive approach to assess the significance of input variables of the SVM model using the Monte Carlo simulation technique. The proposed methodology involves training an SVM model and conducting Monte Carlo

simulations to estimate the significance of the model's input variables, as indicated in the flow chart below.

Let us consider $X$ is a set of input variables such as $X = \{X_1, X_2, X_3, \ldots, X_c\}$ and the significance of the input variable on the output variable(s) is to be investigated. The variable significance analysis of $X_1$ on the output variable by Monte Carlo technique requires varying the operating values of the considered variable from its minimum to maximum value on the introduced step-sizes (m). For each step size taken for $X_1$, several operating values of other variables, i.e., $X_2, X_3, \ldots, X_c$ are randomly generated within their operating bounds. Thus, number of simulated experiments for each step size of $X_1$ are constructed and the procedure is repeated for all the introduced step sizes. This results in the formation of a large number of simulated experiments covering the systematic variation in $X_1$ and the experiments are simulated from the trained ML model. The change in the output variable produced due to $X_1$ is recorded and the procedure is repeated to investigate the change in the output variable due to the remaining input variables ($X_2, X_3, \ldots, X_c$). The change produced in the output variable is normalized to estimate the relative percentage significance of the input variables on the output variables. More details about the Monte Carlo technique-based significance analysis can be reported in [50, 51]. The flow chart of the proposed SVM modeling integrated with Monte Carlo simulations for predicting the performance of the investigated WCSAC is clearly demonstrated in Fig. 3.

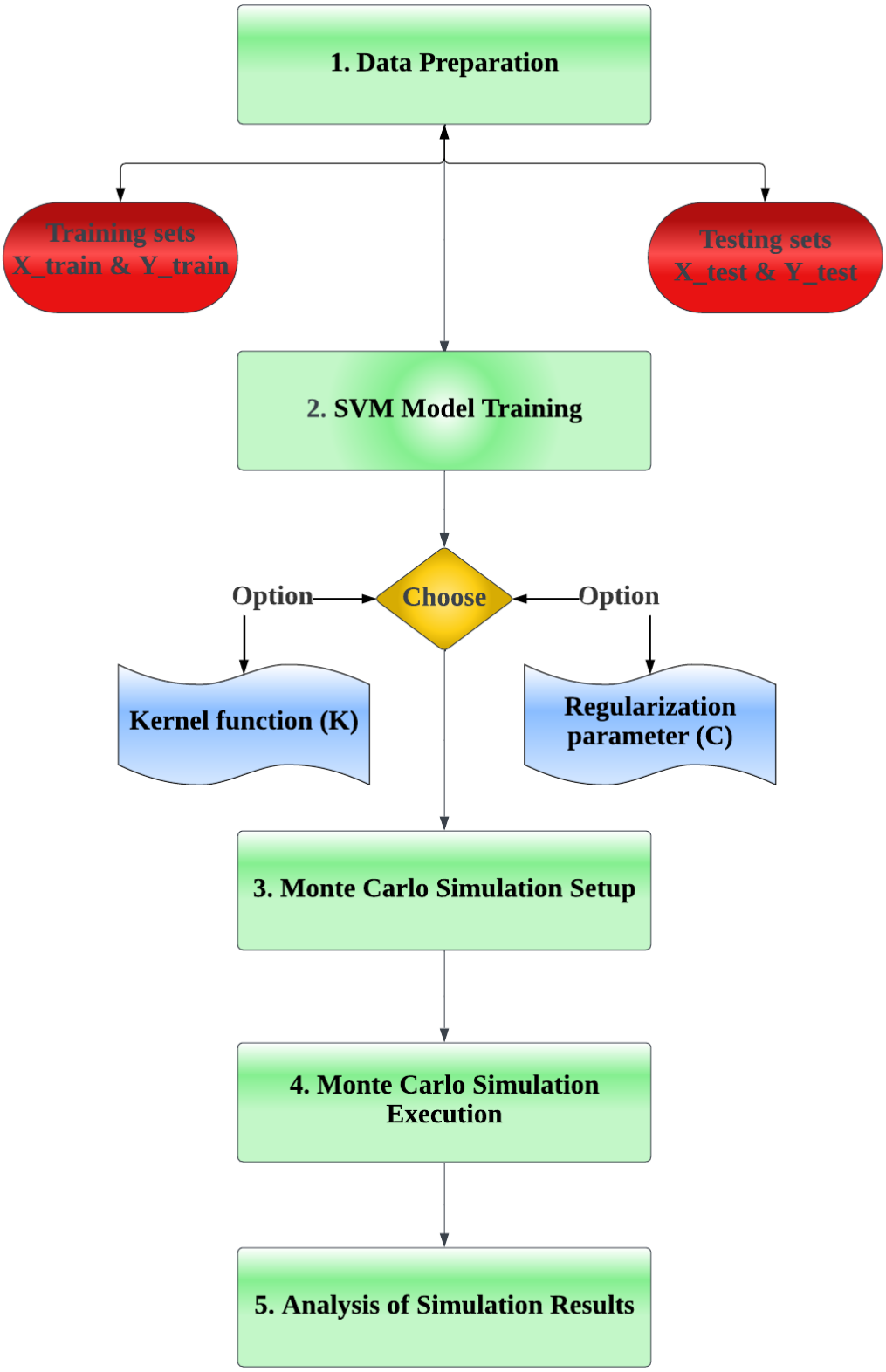


Fig. 3. Flow chart of the proposed SVM modeling integrated with Monte Carlo simulations.

## 4. Results and discussion

This section investigates the performance of wavy-corrugated solar air collector (WCSAC) with and without PCM at various air flow rates of 3.72, 1.68, and 0.54 kg/min. Performance is investigated in terms of temperature, useful heat gain, convective heat transfer coefficient, energy, and exergy parameters. All experiments are carried out with a thickness of PCM of 4 cm and 2 cm rear of the absorber plate of WCSAC on consecutive days under sunny weather conditions in Tanta, Egypt.

### 4. 1 Comparative experimental analysis of the WCSAC with and without PCM

Figure 4 (a) and (b) presents the solar radiation and temperature profile of various components of the proposed WCSAC with and without PCM at a 1.68 kg/min air flow rate in Tanta City Egypt. Firstly, it is declared from Fig. 4 (a) that the behavior of the temperature profile of all elements of WCSAC without PCM follows the behavior of the solar radiation throughout the daylight from 8:00 am to 16:30. The elements' temperature gradually increased with the increase of solar radiation until it reached its peak at 12:30 pm, where the temperature of the absorbent, air outlet, glass plate, and ambient are recorded 77.5, 65.5, 51 and 40°C, respectively, at solar radiation of 980W/$m^2$ during summer climate conditions in Tanta city, Egypt. Secondly, the effect of using PCM on the elements' temperature of WCSAC can be observed in Fig.4 (b). It is seen that without using PCM, the measured exit air temperature of the WCSAC follows the solar intensity as it increases gradually to reach its peak values at noon and then starts to decrease gradually to equal ambient at sunset as shown in Fig. 4 (a). Whereas, from the results of Fig. 4 (b), the PCM melting process starts at 1:30 pm when the temperature of the PCM reaches 54 ºC. Part of absorbed solar energy is stored within the PCM during the melting process at a constant melting temperature of 54 ºC. This stored energy is recovered after 4:30 pm when the sun begins to fade and the mean PCM temperature is higher than the wavy corrugated surface temperature (discharging process). So, the outlet air temperature remains higher than the ambient temperature for many hours after sunset. It is found that the maximum temperature of the PCM is recorded at 60°C at 15:00, which means the end of the heat absorption phase and the start of the heat release phase, resulting in the outlet air temperature remaining 1.5-8°C higher than the ambient temperature within 3.5 h after sunset.

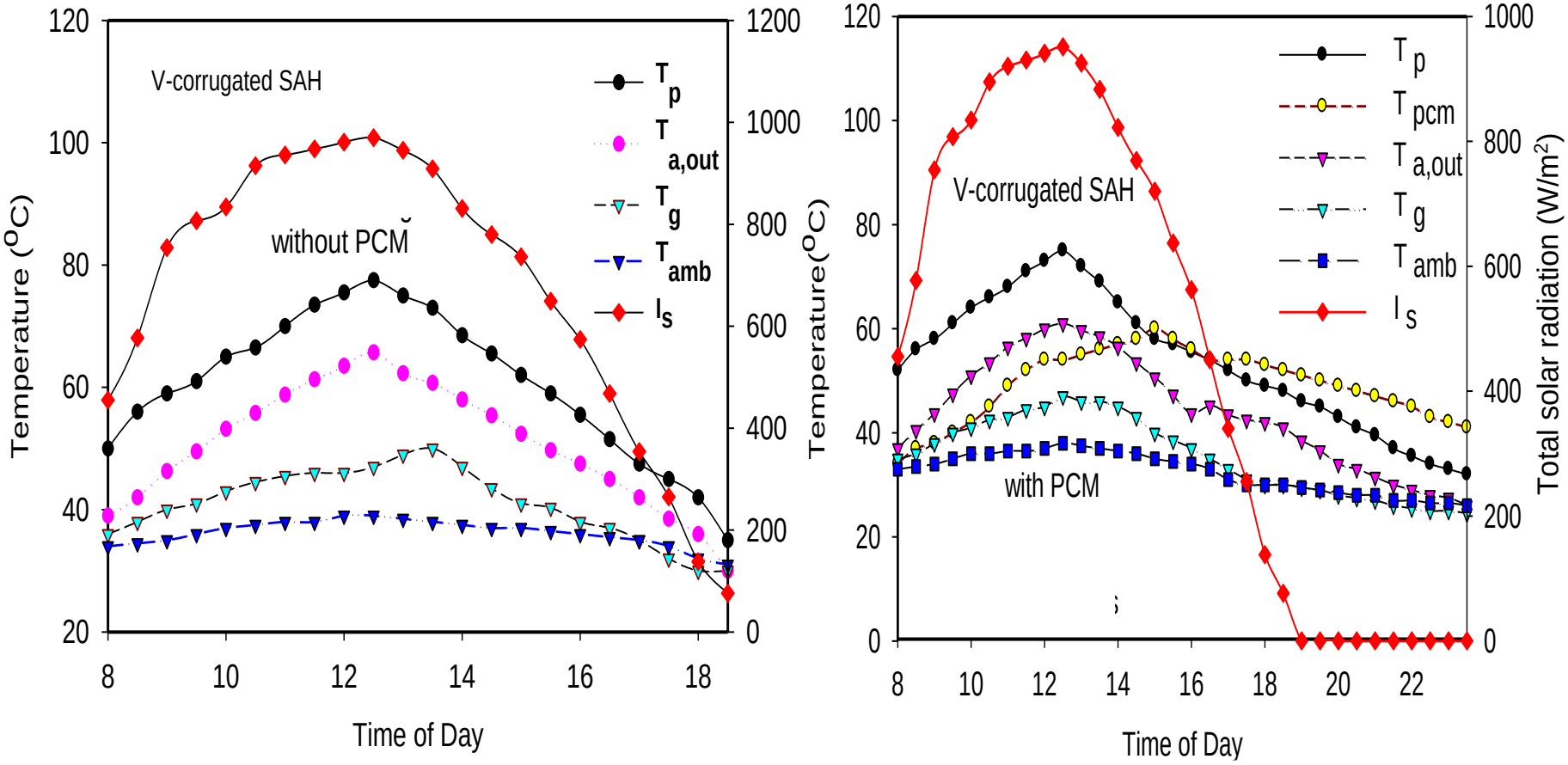


Fig. 4. Temperature profiles of the different components of the proposed WCSAC at an air flowrate of 1.68 kg/min: (a) Without using PCM; (b) With using PCM

Figure 5 illustrates the effect of airflow rates on WCSAC's useful heat gain with and without PCM. The investigation is performed at airflow rates of 0.54, 1.68, and 3.72 kg/min over 24 hours. It is noted that the supply period of WCSAC's useful heat with PCM significantly outperformed WCSAC without PCM at all airflow rates, while the value of WCSAC's useful heat gain without PCM slightly outperformed WCSAC with PCM at all daytime airflow rates. At peak time, the useful heat gain of WCSAC without PCM is 700, 600, and 280 W at airflow rates of 0.54, 1.68, and 3.72 kg/min, respectively, while the useful heat gain of WCSAC with PCM was 100 W less at 3.72 and 1.68 kg/min and 50 W less at 0.54 kg/min. This temperature decrease of WCSAC with PCM indicates that the PCM is in the thermal storing stage or transition to melting (absorbing phase), which requires a large amount of fusion heat, decreasing the useful heat gain of air. It can be noted that the absorbing phase period of PCM starts from 8:00 am till 16:30. The heat stored in PCM can be evaluated after 16:30, when the heat recovery phase (release phase) begins, which peaks around 18:00 (at sunset). The maximum useful heat gain in the releasing phase reached around 700, 300, and 100 W at airflow rates of 3.72, 1.68, and 54 kg/min, respectively, while the WCSAC without PCM achieved zero useful heat. Regarding the heat recovery time, the lowest air flow rate (0.54 kg/min) achieved the longest period, reaching 13 h, then 1.68 kg/min by 10h and 3.72 kg/min by 5h. The change in heat recovery time is expected because the air flow rate is a function of the useful heat gain equation.

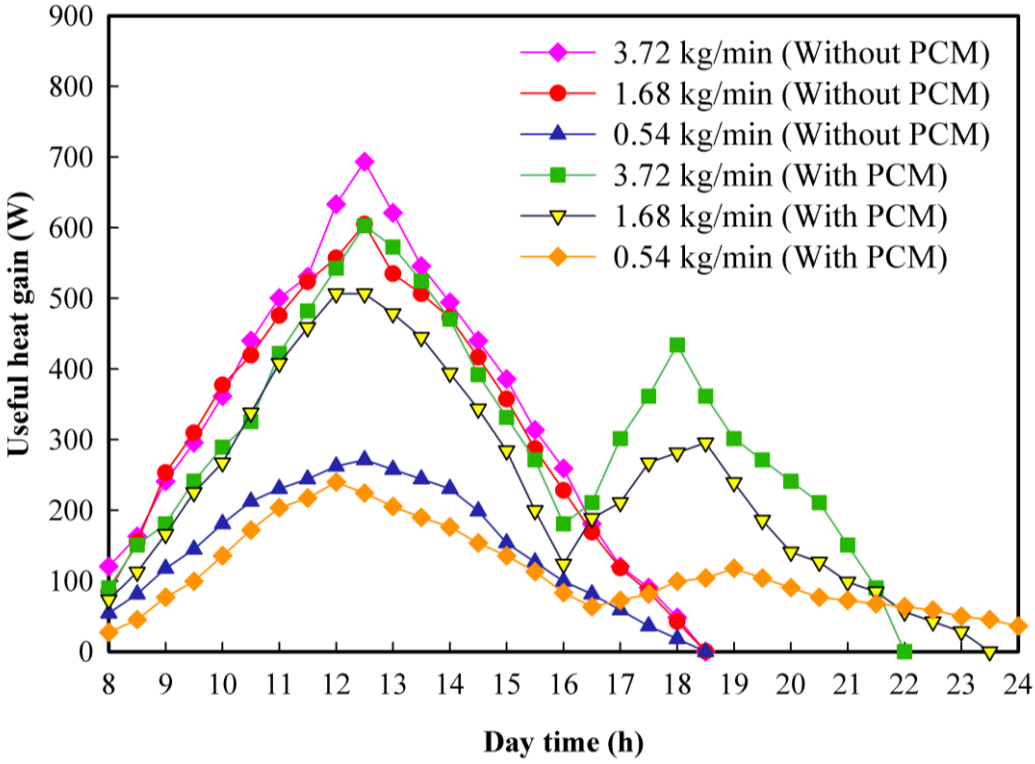


Fig. 5. Variations in the useful heat gain of the WCSAC without and with PCM at several air flowrates.

Figure 6 compares the air temperature difference of WCSAC with and without PCM at airflow rates of 0.54, 1.68, and 3.72 kg/min, at a PCM layer of 4 cm. In the daytime, it can be seen that the heat storage of the PCM has a key influence on the air temperature difference, especially at peak time, as the average temperature difference of a WCSAC without PCM over a WCSAC with PCM increased by 5, 4, and 3°C at an airflow rate of 0.54 and 1.68 and 3.72 kg/min, respectively. It is also noted that the temperature difference values are negatively affected by increasing air flow rate across both WCSACs, with the highest temperature differences for WCSAC without PCM reaching 29°C, 22°C, and 13°C at air flowrates of 0.54, 1.68, and 3.72 kg/min, respectively. This behavior can be interpreted by the fact that the low flow rate means an increase in the contact period of the air mass passing through the wavy-corrugated surface of the solar heater, which allows the air molecules to heat up faster and thus increase the temperature difference. On the contrary, an increase in the flow rate means a shorter time and a decrease in the number of air molecules in contact with the corrugated surface, thus heating the air less and, thus, a smaller temperature difference.

On the other hand, the useful heat gain in Fig. 5 and the heat transfer equation indicate that the temperature difference is conversely proportional to the air flowrate at the same heat gain value. In this context, the temperature difference behavior of WCSAC can be explained

with PCM after sunset (release phase), where the higher air flow rate achieved the lowest temperature difference and shorter recovery period. The lower airflow rate achieved the highest temperature difference and the longest heat recovery duration. The maximum temperature difference through the recovery period (release phase) reached 13.0, 10.5, and 7.2°C through the recovery period of 7.5, 5.0, and 3.5h, respectively.

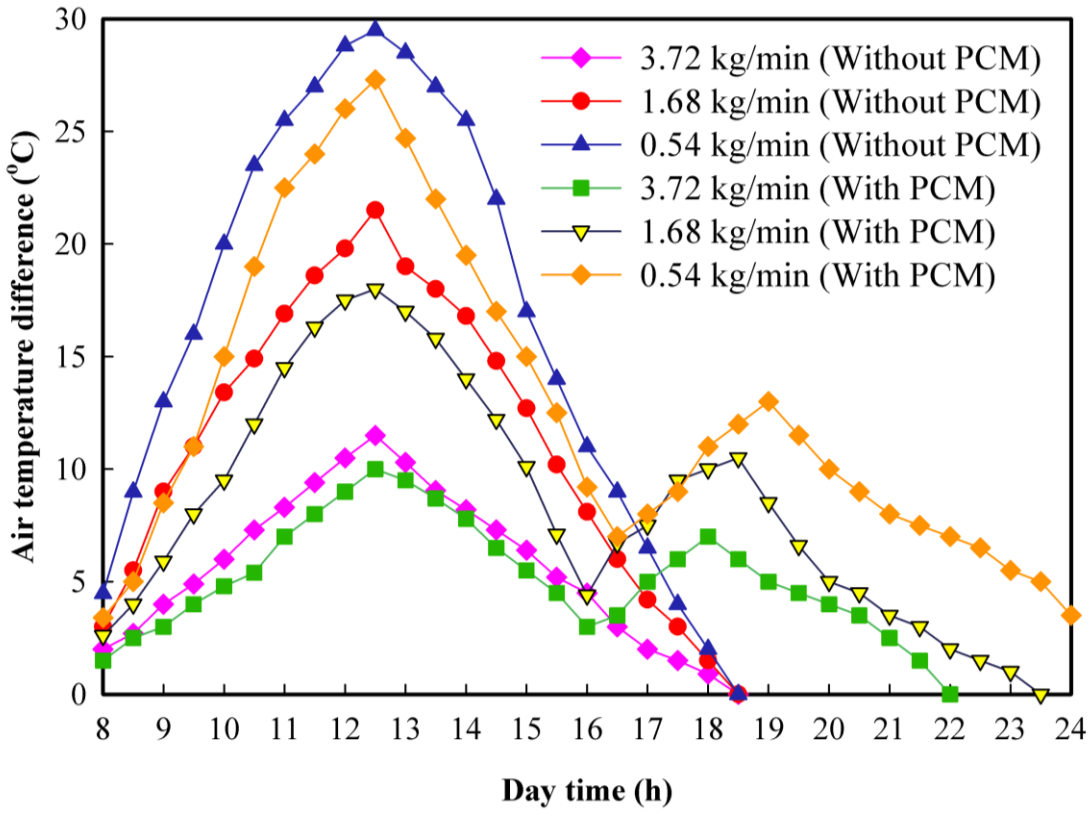


Fig. 6. Variation in the air temperature difference of the WCSAC without and with PCM at several air flowrates at 4 cm PCM layer thick.

The influence of air flowrate on the convective heat transfer coefficient (CHTC) for WCSAC with and without PCM is presented in Fig. 7 when the PCM layer deepness is 4 cm below the absorbent. In general, CHTC is observed to be positively affected by an increase in air flow rate for both WCSACs. This is because the airflow rate directly affects the amount of heat transferred between the wavy-corrugated surface and the air passing through it, as shown in Fig. 5. An increase in the flow rate results in larger velocity and turbulence of the passing air, resulting in better mixing and enhanced contact of the flowing air with the wavy-corrugated surface, which results in more efficient heat transfer. Therefore, an increment in the flow rate leads to an increase in the CHTC. Conversely, at lower flow rates, the fluid near the corrugated surface can become stagnant, creating a boundary layer that slows heat transfer. Thus, increasing the flow rate breaks up this boundary layer and promotes better heat transfer. It is

also notable that the CHTC of the WCSAC with PCM is lower than that of one's free of PCM during the diurnal times from 8:00 am to 16:00. This is because the PCM is in a thermal storage process (absorption phase), which means that the net solar energy of a WCSAC with PCM is transferred in two directions, one for passing air and the other for the PCM, while all the net solar energy of WCSAC free of PCM is transferred to the passing air, which strengthened CHTC. In the daytime, the CHTC for WCSAC without PCM achieved 30, 22.5, and 18 W/m$^2$.℃, while the CHTC for WCSAC with PCM achieved 27.22 and 11.5 W/m$^2$.℃ at the same air flow rate of 3.72, 1.68, and 0.54 kg/min, respectively. In the night period, the CHTC for WCSAC with PCM maxed out at 30, 19, and 10 W/m$^2$. ℃, at a recovery period of 7.5, 5, and 3.5 hours, respectively, at the same airflow rates for the daytime period. It is drawn that the maximum increment in the average CHTC of the WCSAC integrated with PCM is more than 1.20 times that yielded with the WCSAC without PCM.

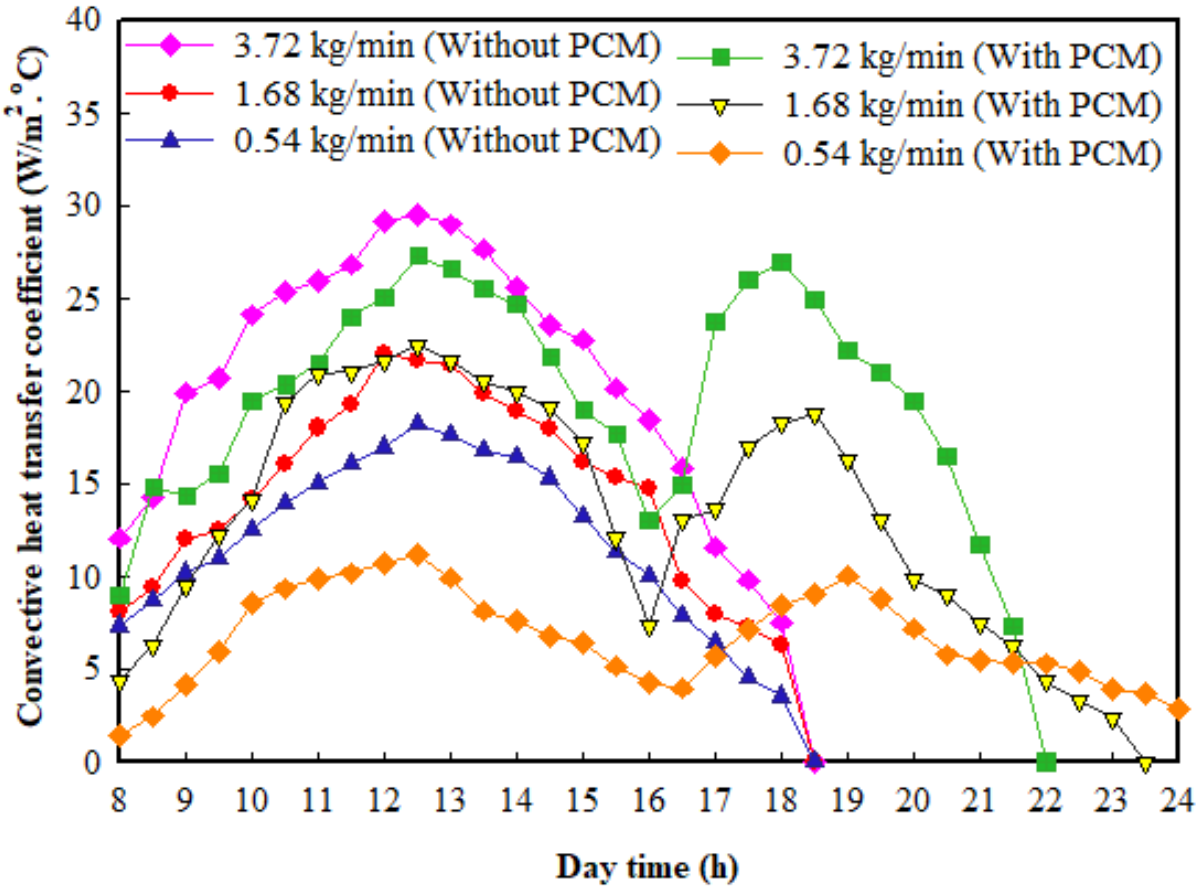


Fig. 7. Changes in the CHTC of the WCSAC without and with PCM at several air flow rates at 4 cm PCM layer thick.

In order to identify the impact of the paraffin layer thickness, the WCSAC is also tested when the PCM thickness is adapted to 4 and 2 cm. Figure 8 illustrates the influence of varying the

thickness of the PCM layer on the hot air temperature of the WCSAC under the investigated different air flowrates when the PCM thickness is adapted 4 and 2 cm. The findings declared that when the thickness of PCM reduces from 4.0 cm (38 kg paraffin wax) to 2.0 cm (19 kg paraffin), the air temperature through the WCSAC increases during the PCM charging process period, after that, it reduces during the discharging process period and engrosses for various fewer hours after the evening time. Due to the decrement in the stored energy rates as the PCM mass is reduced. It is inferred that when the usage of a 2 cm PCM layer thick, the exit air temperature of the WCSAC is higher than the surrounding temperature by 1.75–8.80 °C during 4 h after evening time compared with 2–10.5 °C during 5 h after evening time when 4 cm PCM layer is utilized at the same air flowrate of 1.68, respectively.

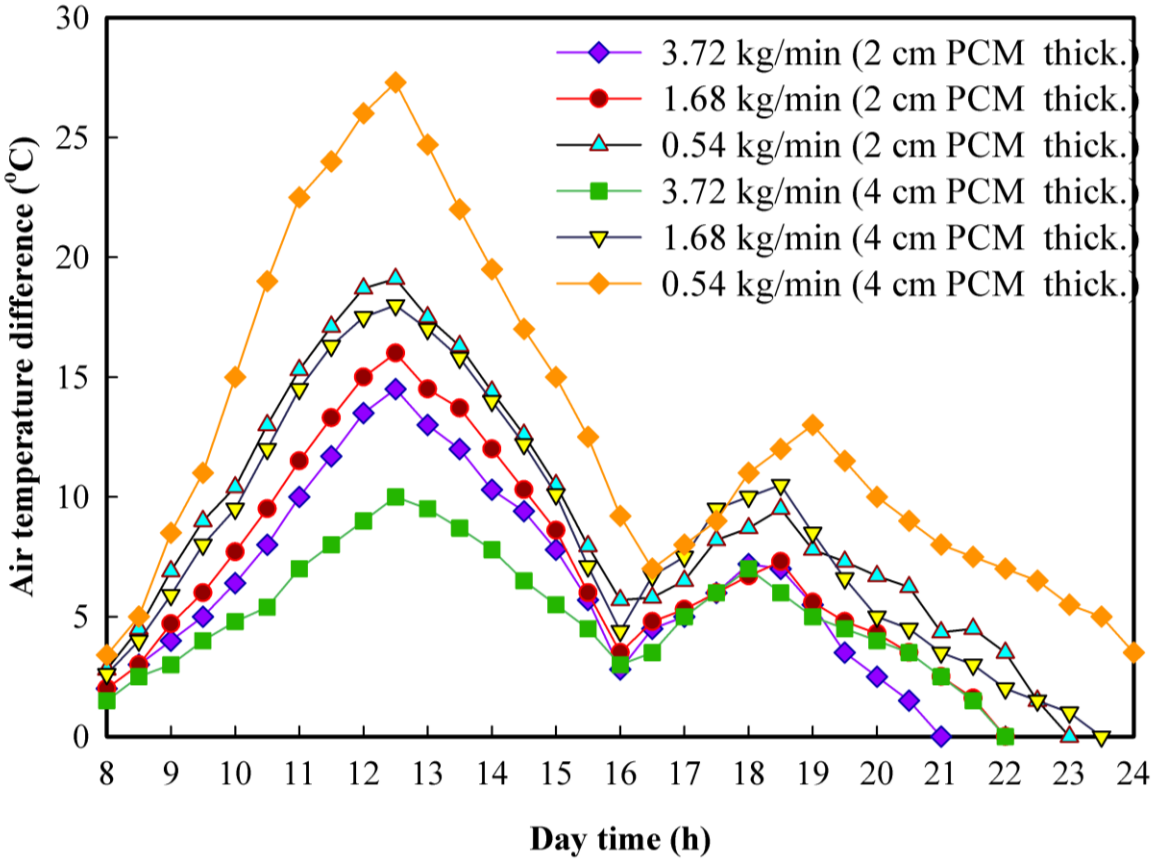


Fig. 6. Variation in the air temperature difference of the WCSAC without and with PCM at several air flowrates at 4 cm and 2 cm PCM layer thick

Energy and exergy efficiency are indispensable considerations for evaluating the performance of such solar thermal systems. Exergy measures useful energy available from the system, while energy efficiency measures the amount of input required for a given output. Regarding WCSACs, exergy determines how much usable thermal energy can be extracted from sunlight, while energy efficiency reflects how effectively this thermal energy is converted into useful

work. Therefore, the exergy and energy efficiency of both WCSACs are investigated to get the maximum thermal benefits from the investment in the SACs. In this context, Fig. 9 charts the daily exergy efficiency of WCSAC with and without PCM at various air flow rates. It can be observed that energy efficiency improves with increasing air flow rate, with PCM-containing WCSAC outperforming its PCM-free counterpart. The daily exergy efficiency of WCSAC with PCM reached 9.90 %, 8.60%, and 5.58% compared to 5.99%, 5.75%, and 5.10% for its PCM-free counterpart at airflow rates of 3.72, 1.68 and 0.54 kg/min, respectively. This result indicates that the exergy efficiency is enhanced by 65.3%, 49.56%, and 9.43% using the PCM at rates of 3.72, 1.68, and 0.54 kg/min airflow, at 4 cm PCM thickness, respectively. Thus, it can be concluded that optimum WCSAC performance can be obtained using PCM with a high airflow rate.

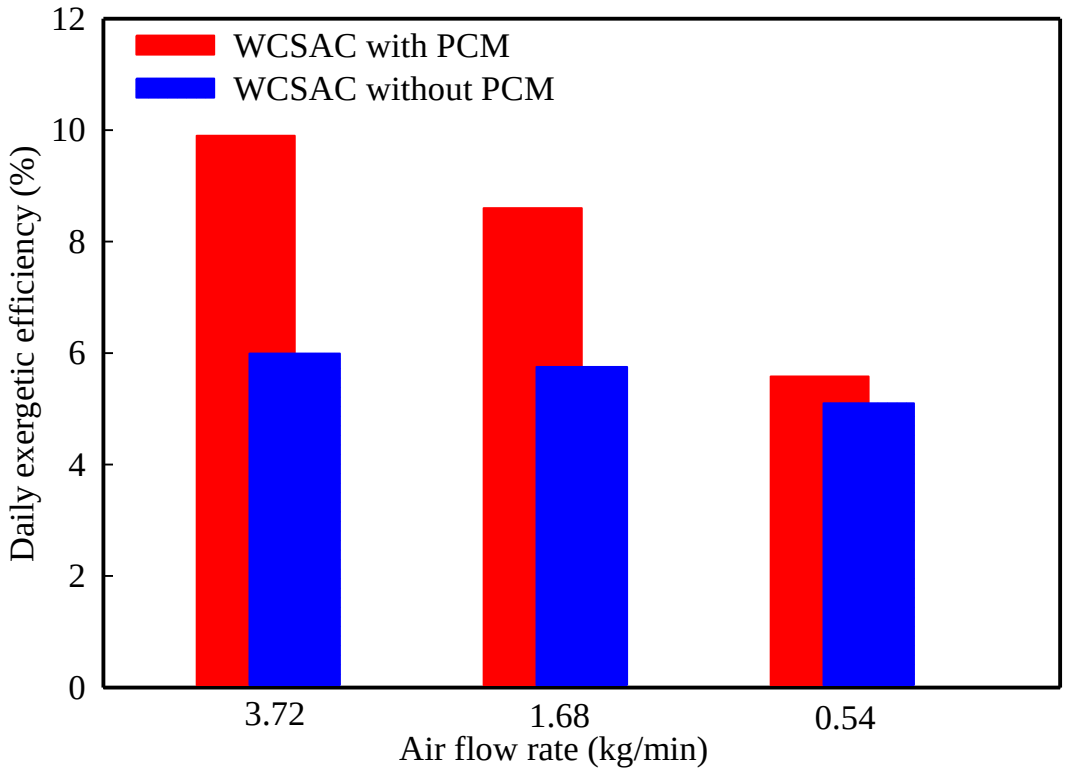


Fig. 9. Changes in the daily exergy efficiency of the WCSAC with and without PCM versus air flowrate.

Figure 10 compares the daily energy efficiency of WCSAC without and with PCM at the same mass flow rates used (0.54, 1.68, and 3.72 kg/min), at 4 cm PCM layer thickness. In general, it can be seen that the energy efficiency is directly proportional to the airflow rate for both WCSACs, since the useful heat gain at high flow rates is higher than at low flow rates, as the heat loss at high flow rates is less than at low flow rates. Also, it is noted that the efficiency of WCSAC with PCM significantly outperforms the efficiency without PCM, where the

WCSAC with PCM achieved 62%, 52%, and 27%, while WCSAC without PCM achieved 50%, 43.2%, and 22.2% at airflow rates of 3.72 and 1.68 and 0.54 kg/min, respectively. Thus, the superiority of WCSAC with PCM over WCSAC without PCM was assessed as 24.0%, 20.39%, and 16.37% at airflow rates of 3.72, 1.68, and 0.54 kg/min, respectively. This superiority indicates that the use of PCM contributes to the storage of a large amount of solar energy and saves it from dispersion and loss; moreover, the PCM provides the advantage of the night use of hot air. Conclusively, the latest outputs infer that combining a wavy-V-shaped corrugated absorbing plate with a paraffin wax latent storage container is a businesslike option for the performance augmentation of solar air collectors for drying utilities.

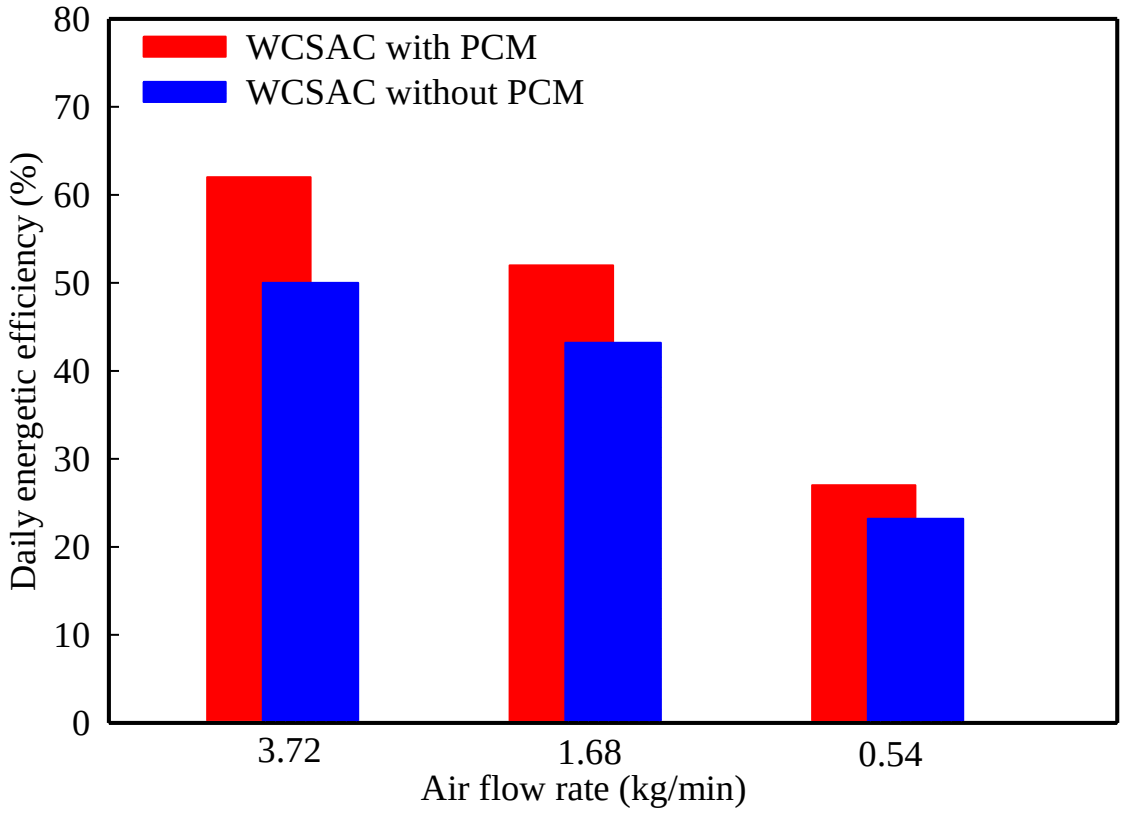


Fig. 10 Variations in the daily energy efficiency of the WCSAC with and without PCM versus air flow rate.

The thermohydraulic performance of the suggested WCSAC with and without PCMs is assessed by means of the thermohydraulic efficacy of the system. This performance indicator is represented as the actual beneficial heat gain by the flowing air considering the pumping power and frictional pressure loss required to propel air via the WCSAC to the incident solar input. A comparison between the daily mean thermohydraulic effectiveness of the WCSAC with and without PCM for multiple values of air flowrates is depicted in Fig. 11. It is revealed that the

WCSAC using PCM yielded comparatively higher thermohydraulic effectiveness at all air flowrates compared to the WCSAC without a PCM. The upcoming finding is because of the predominance of heat transfer enhancements resulting from the implementation of PCM storage over the frictionally pressure drop influences of the airflow over the wavy corrugated absorbent, which the subsequent pressure drop in the WCSAC is influenced marginally by the effective daily energy gain from the collector. It is declared that the daily mean thermohydraulic efficiency values are computed as 58.29%, 49.11%, and 25.65% for the PCM storage-based WCSAC and 47.75%, 41.30%, and 22.35% for the WCSAC without the usage of PCM when the airflow rates are 3.72 and 1.68 and 0.540 kg/min, respectively, at 4 cm PCM layer thickness. Therefore, the outcomes presented in Fig. 11 proved that the thermohydraulic efficacy of the WCSAC with PCM is 22.07%, 18.88%, and 14.76% higher than that of the WCSAC without PCM at airflow rates of 3.72, 1.68, and 0.540 kg/min, respectively.

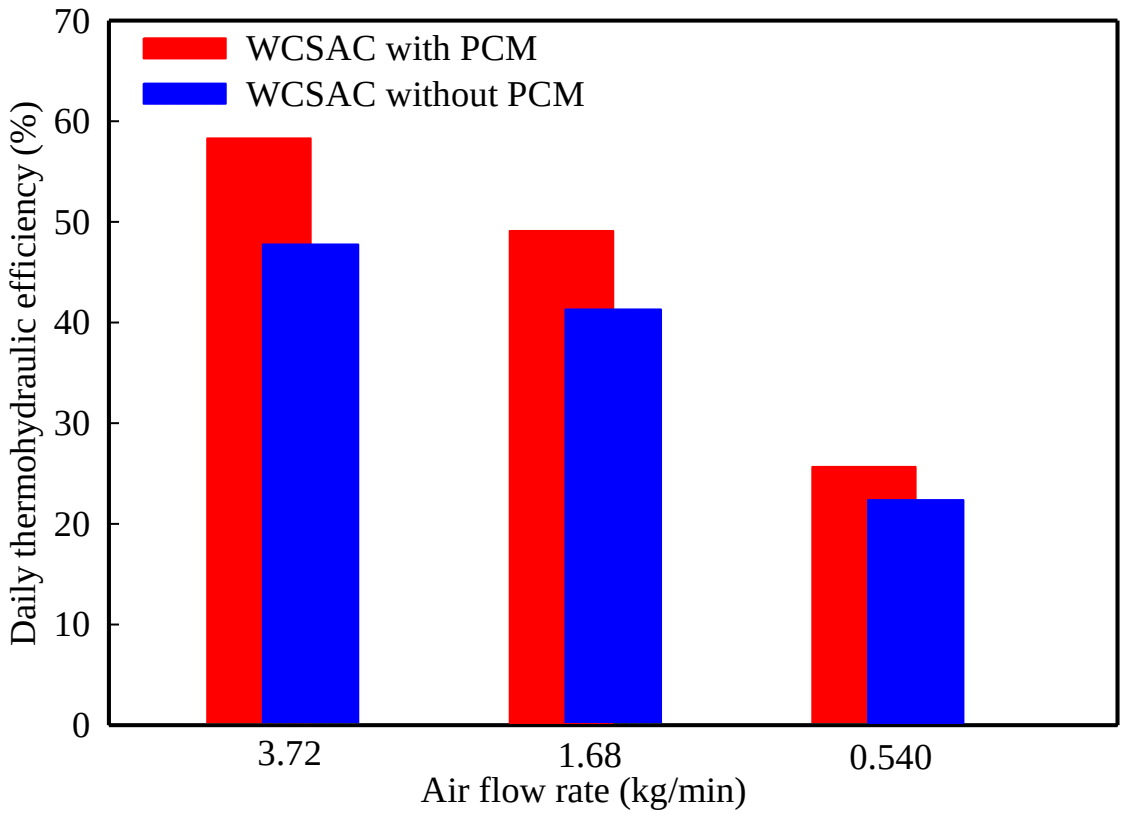


Fig. 11 Variations in daily thermohydraulic efficiency of WCSAC with and without PCM versus air flow rate.

### 4.2 Predictive performance of the developed SVM models

In this paper during the simulations, 132 input-output conditions compiled by simulating the first-principle model are deployed for the training of SVM models. The time, solar radiation, ambient temperature, air inlet temperature, air flowrate, and PCM thickness are used as input

parameters to model and predict the performance outputs of the WCSAC using PCM; including, air temperature ratio, average air temperature, useful heat gain, convective HTC and thermal efficiency by SVM models. For this purpose, a five-fold cross-validation technique is implemented to achieve good generalization performance of the SVM models and overcome the overfitting problem within the suggested SVM model. Furthermore, rigorous hyperparameters associated with the SVM model are tuned iteratively to minimize predictive error. Different kernel functions like quadratic, cubic, and Gaussian are tried, and a large operating range of epsilon ($\varepsilon$) and box constraint ($C$) is investigated as well as the optimal value of these hyperparameters are found by Bayesian optimization and expected improvement per second plus technique. The optimized values of the hyperparameters can improve the predictive performance of the SVM model [52, 53].

Figure 12 presents the predictive performance of the trained SVM models for the output variables. The $R^2$ value for the air temperature ratio is 0.92 signifying good predictive accuracy of the model. Whereas, RMSE is 0.05 which is fairly small in the predictions of the model. Similarly, the $R^2$ value for the four output variables namely average air temperature, useful heat gain, convective HTC, and thermal efficiency is equal to or more than 0.88 and RMSE is 2.2, 35.2, 0.54, and 21.4 respectively demonstrating good functional mapping among the output variables. The performance metrics for the trained SVM models are reasonably good to ensure the excellent modelling and predictive performance of the models on the conditions of input variables.

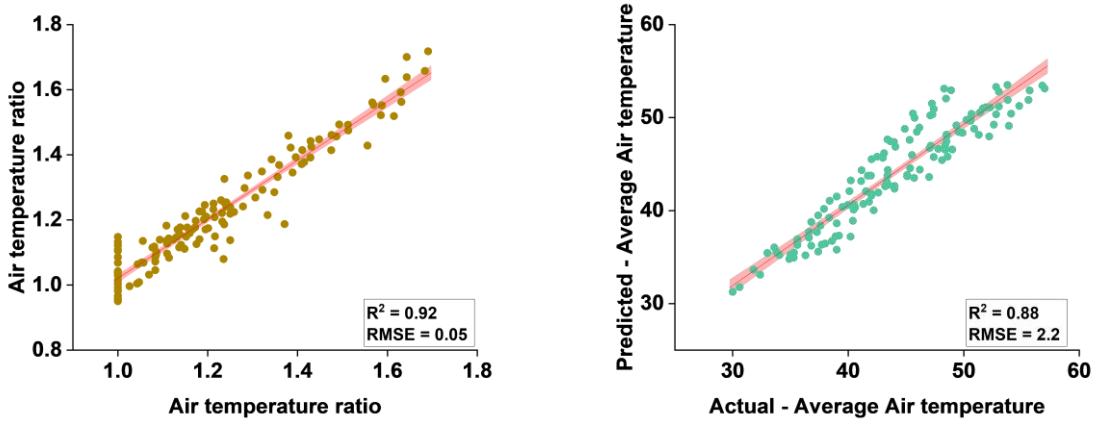

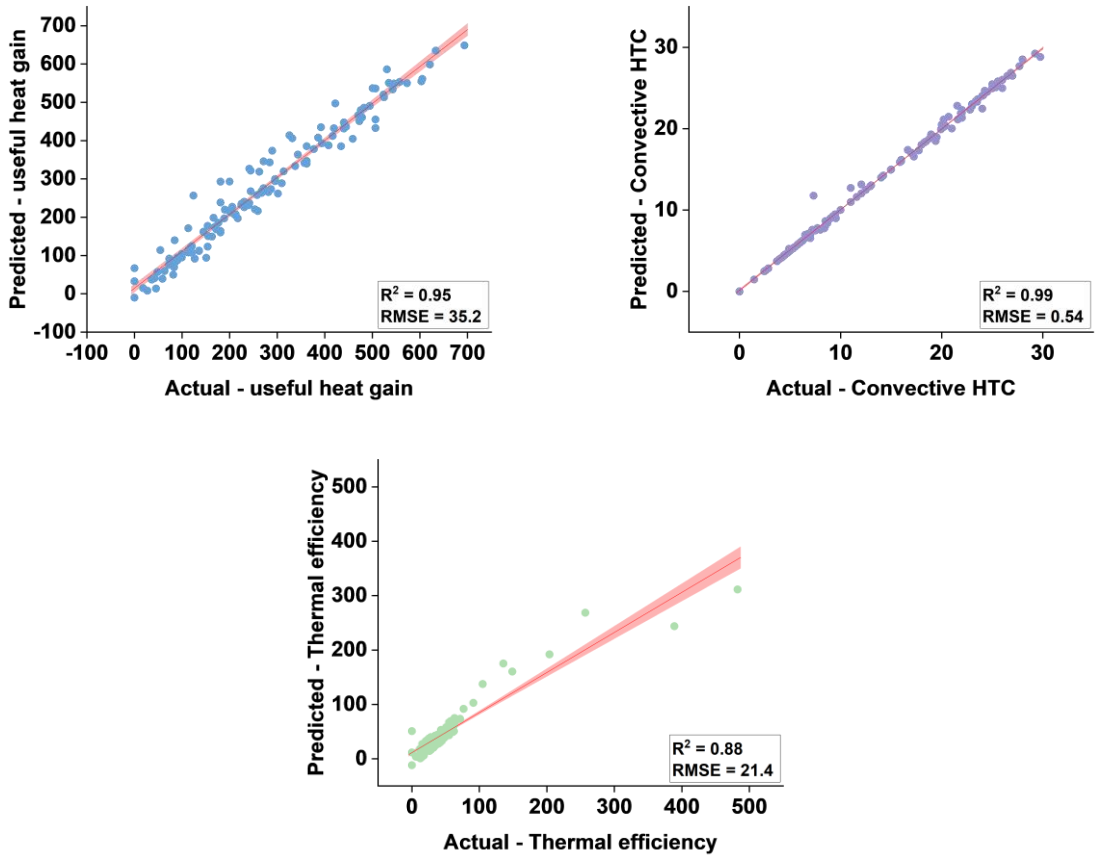


Figure 12. Predictive performance of SVM models for air temperature ratio, average air temperature, useful heat gain, convective HTC, and thermal efficiency of the WCSAC with PCM.

### 4.3 Significance of input variables toward the predicted outputs using Monte Carlo simulation

In this work, 1000 observations are generated from the operating range of the input variables for carrying out Monte Carlo technique-based sensitivity analysis [50, 54]. During the simulations, ten divisions in the operating range of the variable, whose significance is to be evaluated, are made. This results in the construction of 10100 simulated experiments for the comprehensive evaluation of the variables' significance towards the output variable. The mean and standard deviation in the model predictions with respect to the considered input variable are calculated and the confidence bounds are constructed on a 95% confidence interval.

Figure 13 presents the SVM models-based percentage significance of the input variables as computed by the Monte Carlo technique for air temperature, average air temperature, useful heat gain, CHTC, and thermal efficiency. Ambient temperature is termed to be the most significant input variable towards air temperature with a percentage significance of 23.1 ± 7.5. The significance order of the remaining input variables towards the air temperature ratio is as

follows: air inlet temperature = 20.8 ± 6.0, solar radiation = 20.7 ± 8.1, PCM thickness = 12.1 ± 8.4, mass flow rate = 12.1 ± 4.2, and time = 10.9 ± 1.0. Similarly, solar radiation, air inlet temperature, time, PCM thickness, ambient temperature, and airflow rate are arranged from most significant to least significant input variables towards average air temperature and their percentage significance values are as follows: 47.4 ± 3.0, 24.0 ± 11.2, 19.5 ± 14.8, 12.1 ± 1.4, 5.5 ± 3.1, and 0.8 ± 0.2 respectively.

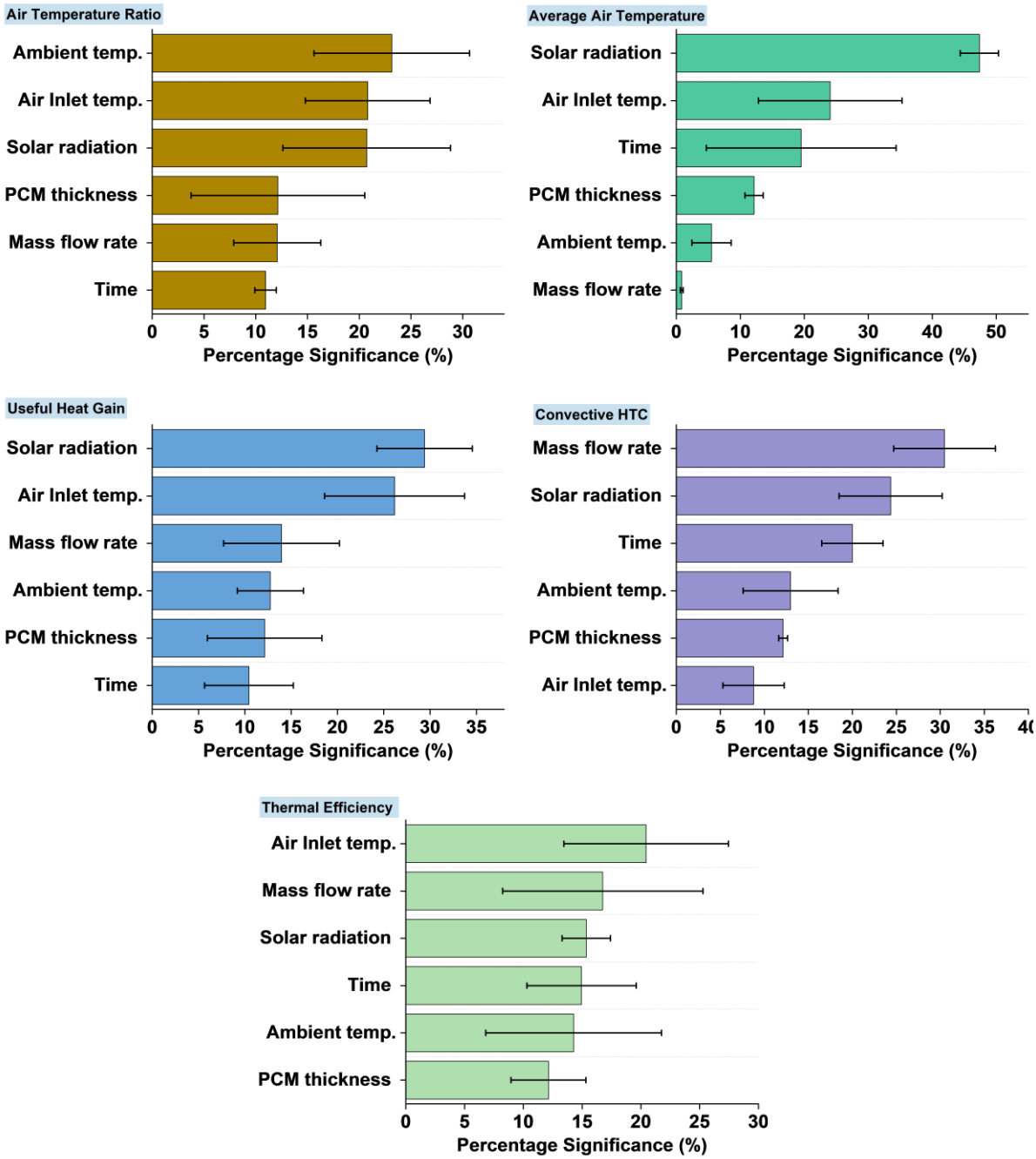


Fig. 13 Monte Carlo technique-based input variables' significance towards the prediction of output variables.

## 5. Economic analysis

The economic analysis of a wavy corrugated solar air collector (WCSAC) is essential for evaluating the long-term financial viability and potential benefits of implementing such a system. The economic analysis of these solar air heaters is performed based on the following parameters [55]

The yearly cost (*YC*) of the WCSAC per unit area can be evaluated by considering the yearly capital cost (*YCC*), yearly pump cost (*YPC*), yearly salvage value (*YSV*), and annual maintenance cost (*YMC*), which can be written as [55];

$$YC = YCC + YPC + YMC - YSV \tag{30}$$

5.1 Annual capital cost

The yearly capital cost is an important parameter to consider when evaluating the solar air collector cost. It considers all investments in physical assets, such as materials, structures, and manufacturing. Hence, it provides valuable information for investment in corrugated solar air collectors. It can be calculated as;

$$YCC = IC \times CRF \tag{31}$$

$$CRF = \frac{i(1+i)^n}{(1+i)^n - 1} \tag{32}$$

Where *IC* describes the initial capital, which consists of the cost of material, fabrication, paint, and absorber plate. Whereas *CRF* is the capital recovery factor, including the interest rate (*i*) and the solar air heater lifespan years (*n*).

5.2 Annual pumping cost

The yearly pumping cost for these systems is typically much lower than traditional heating sources such as gas or electric furnaces, which can be calculated as;

$$APC = \frac{\dot{m}\,\Delta P}{\rho}\, t_{op}\, EC \tag{33}$$

*Where* $\rho$, $\dot{m}$, and $\Delta P$ are the air density, mass flow rate, and pressure drop, respectively, while the $t_{op}$ is the running time, and *EC* is the electricity cost.

5.3. Annual salvage

The yearly salvage cost of the solar air collector can be calculated as;

$$ASV = SFF \times SV \tag{34}$$

Where *SFF* and SV are the salvage fund factor and salvage valve, which are given as;

$$SFF = \frac{i}{(i+1)n - 1} \tag{35}$$

$$SV = 0.1 \times IC \tag{36}$$

5.4 Annual useful energy

The yearly useful energy (*YUE*) is an assessment of the amount of energy the WCSAC can harvest from the sun during the year

$$YUE = S \times A_b \times N_d \times N_h \times \eta \quad (37)$$

*Where S is solar radiation* incident on the WCSAC by W/m$^2$, $A_b$ is the wavy corrugated solar area by m$^2$, $N_d$ is the number of sunny days, $N_h$ is the operating hours' number per day, and $\eta$ is the energy efficiency. Hence, it can be calculated the useful energy cost per kWh as follows;

$$Cost\ of\ useful\ energy = \frac{YC}{YUE} \quad (38)$$

The fixed cost of the components and economic analysis findings of the fabricated WCSAC are highlighted in Table 4. The findings show that the cost of one kW is 0.0112 $/kWh. It can be noted that this technology provides significant savings in terms of operational costs compared with traditional energy sources such as coal or natural gas.

**Table 4.** Costs estimation and economic analysis findings.

| **Parameter** | **Value** |
|---|---|
| Cost of wavy corrugated copper absorber, ($) | 55 |
| Cost of glass cover, ($) | 10 |
| Cost of 38 kg paraffin wax, ($) | 20 |
| Cost of small-scale air blower, ($) | 25 |
| Thermal foam insulation, ($) | 5 |
| Connection pipes and valves, ($) | 10 |
| Paint and silicon, ($) | 5 |
| Overall fixed cost, ($) | 130 |
| Lifetime of the system, (yrs) | 25 |
| Number of working days per year (day) | 350 |
| Air flow rate, (kg/min) | 3.72 |
| Annual heat production, (kW/yr) | 2888 |
| Cost of 1 kW of thermal heat gain ($/kW) | 0.0112 |

Finally, it could deduced that the inclusion of the paraffin wax as a PCM with the suggested WCSAC is an efficient strategy to augment the energetic, thermohydraluic, and exergetic performances of the air solar heaters. For future prospectives, multiobjective optimization studies with in depth exergectic losses considerations of this new WCSAC are highly recommended to identify the desired design and operational parameters (air flowrate, collector dimensions, wave corrugation pitch, PCM type, PCM layer thickness, and PCM melting fraction), which may be optimized the performances of WCSAC. On the other hand, from

machine learning aspects, we plan to expand the dataset to optimize the prediction model, collecting more real-time weather data to further improve prediction accuracy. Moreover, a dynamic seed-bed scheduling scheme is also highly recommended in the future constructed by leveraging a model-based approach and a cloud-edge-end merged cybernetics computing paradigm.

## 6. Conclusions

This study involves an experimental investigation and advanced machine learning modeling to assess the exergy and energy performances of a wavy corrugated solar air collector (WCSAC) embedded with phase change materials (PCM) under diverse operating conditions. For examination of energy and exergy parameters, experiments on the WCSAC were performed under three air flow rates of 0.54, 1.68, and 3.72 kg/min and two PCM layer thicknesses of 2 cm and 4 cm, respectively, and the results compared with those of a WCSAC without using PCM. Moreover, a robust SVM model is developed to predict the performance parameters (air temperature ratio, average air temperature, coefficient of convection heat transfer, and energy efficiency) of the WCSAC with and without the usage of PCM. In addition, a sensitivity analysis is also conducted to explore the significance of model input parameters (air inlet temperature, time, solar irradiance, air flowrate, and PCM layer thickness) on the output parameters prediction using the Monte Carlo simulation technique. The most substantial outcomes reached are as follows:

1. The exit air temperature of the WCSAC using 4 cm PCM layer thickness is higher than ambient temperature by 1.5–7.2 °C during 3.5 h after sunset, 2.0–10.5 °C during 5 h after sunset, and 2–13 °C for 6 h after sunset when the air flowratė is 3.72, 1.68 and 0.54 kg/min respectively.
2. The WCSAC with PCM achieved a daily energy efficiency of 62%, 52%, and 27%, while WCSAC without PCM achieved 50%, 43.2%, and 22.2% at airflow rates of 3.72 and 1.68 and 0.54 kg/min, respectively, at 4 cm PCM layer thickness. Thus, the superiority in energy efficiency of WCSAC with PCM over WCSAC without PCM was assessed as 24.0%, 20.39%, and 16.37% at airflow rates of 3.72, 1.68, and 0.54 kg/min, respectively.
3. The daily exergy efficiencies of the WCSAC equipped with PCM are obtained as 9.90%, 8.60%, and 5.58%, whereas, they are 5.99%, 5.75%, and 5.10% for WCSAC without PCM at airflow rates of 3.72, 1.68 and 0.54 kg/min, respectively. These findings refer to that, the

daily exergy efficiency is improved by 65.3%, 49.56%, and 9.43% for WCSAC with PCM, respectively, w.r.t WCSAC without PCM at airflow rates of 3.72, 1.68, and 0.54 kg/min.

4. The optimal solution of the non-linear dual problem in SVM is developed by incorporating the Karush-Kuhn-Tucker conditions and Lagrangian function kernel function. The developed SVM model shows a superior performance for predicting the performance parameters of the proposed WCSAC with and without using PCM with the highest determination coefficient of 0.990 and 0.950 for training and test processes, respectively.
5. The sensitivity analysis of the input variables as computed by Monte Carlo technique indicates that solar radiation was the most sensitive towards the useful heat gain prediction among all input parameters, followed by air inlet temperature, air flow rate, ambient temperature, and time, respectively. While the PCM thickness was the least sensitive to the system performance outputs.
6. It can be proposed that the utilization of wavy corrugated absorbent integrated with 4 cm paraffin layer thickness represents an effective design configuration for maximization of the heat transfer characteristics and energic-exergic performance of the solar air collectors. It can be deduced that the applicability of the optimized SVM coupled Monte Carlo simulation demonstrates a positive performance for minimizing the computational time required to obtain the optima that are eminently desired not only for solar energy systems but also for most real-time applications.

**References**

[1] G. Palanikumar, S. Shanmugan, V. Chithambaram, S. Gorjian, C.I. Pruncu, F.A. Essa, A.E. Kabeel, H. Panchal, B. Janarthanan, H. Ebadi, A.H. Elsheikh, P. Selvaraju, Thermal investigation of a solar box-type cooker with nanocomposite phase change materials using flexible thermography, Renewable Energy, 178 (2021) 260-282.
[2] A. Khelifa, A.E. Kabeel, M.E.H. Attia, M.E. Zayed, M. Abdelgaied, Numerical analysis of the heat transfer and fluid flow of a novel water-based hybrid photovoltaic-thermal solar collector integrated with flax fibers as natural porous materials, Renewable Energy, 217 (2023) 119245.
[3] I.G. Energy, CO2 Status Report 2017. International Energy agency. 2017c, in, ed, 2018.
[4] N. Lior, Sustainable energy development: The present (2009) situation and possible paths to the future, Energy, 35 (2010) 3976-3994.
[5] L. Ma, Y. Li, J. Wang, S. Li, J. Zhao, W. Li, M.E. Zayed, Q. Shao, M. Sun, A thermal-dissipation correction method for in-situ soil thermal response test: Experiment and simulation under multi-operation conditions, Energy and Buildings, 194 (2019) 218-231.
[6] R. Almodfer, M.E. Zayed, M.A. Elaziz, M.M. Aboelmaaref, M. Mudhsh, A.H. Elsheikh, Modeling of a solar-powered thermoelectric air-conditioning system using a random vector

functional link network integrated with jellyfish search algorithm, Case Studies in Thermal Engineering, 31 (2022) 101797.
[7] M.M. Aboelmaaref, M.E. Zayed, J. Zhao, W. Li, A.A. Askalany, M. Salem Ahmed, E.S. Ali, Hybrid solar desalination systems driven by parabolic trough and parabolic dish CSP technologies: Technology categorization, thermodynamic performance and economical assessment, Energy Conversion and Management, 220 (2020) 113103.
[8] S. Sadek, S. Deng, J. Zhao, M.E. Zayed, Solar-powered adsorption-based atmospheric water harvesting systems: Principles, materials, performance analysis, and configurations, Sustainable Energy Technologies and Assessments, 54 (2022) 102874.
[9] J. Zhang, T. Zhu, Systematic review of solar air collector technologies: Performance evaluation, structure design and application analysis, Sustainable Energy Technologies and Assessments, 54 (2022) 102885.
[10] S. Shoeibi, H. Kargarsharifabad, S.A.A. Mirjalily, M. Zargarazad, Performance analysis of finned photovoltaic/thermal solar air dryer with using a compound parabolic concentrator, Applied Energy, 304 (2021) 117778.
[11] S.M. Shalaby, A. Khalil, A.E. Kabeel, M.E. Zayed, Improvement of the Thermal Performance of the v-Corrugated Plate Solar Air Heater with PCM by Using Insulated Upper Cover during Night, in: 2018 IEEE International Conference on Smart Energy Grid Engineering (SEGE), 2018, pp. 346-350.
[12] A.E. Kabeel, A. Khalil, S.M. Shalaby, M.E. Zayed, Experimental investigation of thermal performance of flat and v-corrugated plate solar air heaters with and without PCM as thermal energy storage, Energy Conversion and Management, 113 (2016) 264-272.
[13] A.K. Hegde, P. Raghuvir, K.V. Karanth, Performance augmentation of solar air heaters: A comprehensive analysis, Solar Energy, 253 (2023) 527-553.
[14] K. Nidhul, A.K. Yadav, S. Anish, U.C. Arunachala, Thermo-hydraulic and exergetic performance of a cost-effective solar air heater: CFD and experimental study, Renewable Energy, 184 (2022) 627-641.
[15] W.S. Abushanab, M.E. Zayed, R. Sathyamurthy, E.B. Moustafa, A.H. Elsheikh, Performance evaluation of a solar air heater with staggered/longitudinal finned absorber plate integrated with aluminium sponge porous medium, Journal of Building Engineering, 73 (2023) 106841.
[16] A. Arshad, S.A. Iqrar, S.C. Costa Pereira, M.W. Shahzad, K. Nawaz, W. Worek, Cooling performance of an active-passive hybrid composite phase change material (HcPCM) finned heat sink: Constant operating mode, International Journal of Heat and Mass Transfer, 207 (2023) 123973.
[17] K.C. Ng, K. Thu, S.J. Oh, L. Ang, M.W. Shahzad, A.B. Ismail, Recent developments in thermally-driven seawater desalination: Energy efficiency improvement by hybridization of the MED and AD cycles, Desalination, 356 (2015) 255-270.
[18] M.W. Shahzad, K. Thu, Y.-d. Kim, K.C. Ng, An experimental investigation on MEDAD hybrid desalination cycle, Applied Energy, 148 (2015) 273-281.
[19] A.K. Bhardwaj, R. Chauhan, R. Kumar, M. Sethi, A. Rana. Experimental investigation of an indirect solar dryer integrated with phase change material for drying valeriana jatamansi (medicinal herb). Case Stud Therm Eng, 10 (2017), pp. 302-314

[20] Z. Azaizia, S. Kooli, I. Hamdi, W. Elkhal, A.A. Guizani. Experimental study of a new mixed mode solar greenhouse drying system with and without thermal energy storage for pepper. Renewable Energy, 145 (2020), pp. 1972-1984.
[21] M. Abuşka, S. Şevik, A. Kayapunar, A comparative investigation of the effect of honeycomb core on the latent heat storage with PCM in solar air heater, Applied Thermal Engineering, 148 (2019) 684-693.
[22] S. Das, A. Biswas, B. Das, Parametric investigation on the thermo-hydraulic performance of a novel solar air heater design with conical protruded nozzle jet impingement, Applied Thermal Engineering, 219 (2023) 119583.
[23] M.A. Eleiwi, H.S. Shallal, Thermal performance of solar air heater integrated with air–water heat exchanger assigned for ambient conditions in Iraq, International Journal of Ambient Energy, 43 (2022) 2153-2164.
[24] A.D. Tuncer, A. Khanlari, A. Sözen, E.Y. Gürbüz, C. Şirin, A. Gungor, Energy-exergy and enviro-economic survey of solar air heaters with various air channel modifications, Renewable Energy, 160 (2020) 67-85.
[25] A.K. Raj, M. Srinivas, S. Jayaraj, CFD modeling of macro-encapsulated latent heat storage system used for solar heating applications, International Journal of Thermal Sciences, 139 (2019) 88-104.
[26] M.M. Matheswaran, T.V. Arjunan, S. Muthusamy, L. Natrayan, H. Panchal, S. Subramaniam, N.K. Khedkar, A.S. El-Shafay, C. Sonawane, A case study on thermo-hydraulic performance of jet plate solar air heater using response surface methodology, Case Studies in Thermal Engineering, 34 (2022) 101983.
[27] V.D. Nagale, S. Singh, S. Kumar, Design of a recyclic solar air heater for low temperature regions utilizing integrated wavy corrugated thermal energy storage systems, Applied Thermal Engineering, 227 (2023) 120422.
[28] P. Ganesh Kumar, V.S. Vigneswaran, K. Balaji, S. Vinothkumar, R. Prabakaran, D. Sakthivadivel, M. Meikandan, S.C. Kim, Augmented v-corrugated absorber plate using shot-blasting for solar air heater – Energy, Exergy, Economic, and Environmental (4E) analysis, Process Safety and Environmental Protection, 165 (2022) 514-531.
[29] A.S. Kashyap, R. Kumar, P. Singh, V. Goel, Solar air heater having multiple V-ribs with Multiple-Symmetric gaps as roughness elements on Absorber-Plate: A parametric study, Sustainable Energy Technologies and Assessments, 48 (2021) 101559.
[30] K. Nidhul, D. Thummar, A.K. Yadav, S. Anish, Machine learning approach for optimization and performance prediction of triangular duct solar air heater: A comprehensive review, Solar Energy, 255 (2023) 396-415.
[31] H.R. Aidinlou, A.M. Nikbakht, Intelligent modeling of thermohydraulic behavior in solar air heaters with artificial neural networks, Neural Computing and Applications, 31 (2019) 3279-3293.
[32] S.P. Shetty, S. Nayak, S. Kumar, K. Vasudeva Karanth, Thermo-hydraulic performance prediction of a solar air heater with circular perforated absorber plate using Artificial Neural Network, Thermal Science and Engineering Progress, 23 (2021) 100886.
[33] H. Esen, F. Ozgen, M. Esen, A. Sengur, Artificial neural network and wavelet neural network approaches for modelling of a solar air heater, Expert Systems with Applications, 36 (2009) 11240-11248.

[34] S. Erenturk, K. Erenturk, Comparisons of novel modeling techniques to analyze thermal performance of unglazed transpired solar collectors, Measurement, 116 (2018) 412-421.
[35] A. Saravanan, S. Parida, M. Murugan, M.S. Reddy, P.V. Elumalai, S. Kumar Dash, Thermal performance prediction of a solar air heater with a C-shape finned absorber plate using RF, LR and KNN models of Machine learning, Thermal Science and Engineering Progress, 38 (2023) 101630.
[36] M.E. Zayed, V.P. Katekar, R.K. Tripathy, S.S. Deshmukh, A.H. Elsheikh, Predicting the yield of stepped corrugated solar distiller using kernel-based machine learning models, Applied Thermal Engineering, 213 (2022) 118759.
[37] A. Parsaie, A.H. Haghiabi, A. Moradinejad, Prediction of Scour Depth below River Pipeline using Support Vector Machine, KSCE Journal of Civil Engineering, 23 (2019) 2503-2513.
[38] Z. Wang, J. Crook, G. Andreeva, Reducing estimation risk using a Bayesian posterior distribution approach: Application to stress testing mortgage loan default, European Journal of Operational Research, 287 (2020) 725-738.
[39] J. Hill, J. Jenkins, D. Jones, Testing of solar collectors according to ASHRAE Standard 93-77, ASHRAE Journal, 84 (1978) 107-125.
[40] F.A. Hammad, S.M. Shalaby, A.E. Kabeel, M.E. Zayed, Experimental investigation and thermo-economic performance analysis of a modified solar distiller design with thermal storage material and v-corrugated absorber basin, Journal of Energy Storage, 52 (2022) 105020.
[41] J.P. Holman, Experimental methods for engineers, (2012).
[42] E. Vengadesan, R. Senthil, A review on recent developments in thermal performance enhancement methods of flat plate solar air collector, Renewable and Sustainable Energy Reviews, 134 (2020) 110315.
[43] A.A. El-Sebaii, S. Aboul-Enein, M.R.I. Ramadan, S.M. Shalaby, B.M. Moharram, Investigation of thermal performance of-double pass-flat and v-corrugated plate solar air heaters, Energy, 36 (2011) 1076-1086.
[44] K. Vafai, C.L. Tien, Boundary and inertia effects on flow and heat transfer in porous media, International Journal of Heat and Mass Transfer, 24 (1981) 195-203.
[45] M. El Hadi Attia, M.E. Zayed, A.E. Kabeel, A.S. Abdullah, M. Abdelgaied, Energy, exergy, and economic analyses of a modified hemispherical solar distiller augmented with convex absorber basin, wicks, and PCM, Solar Energy, 261 (2023) 43-54.
[46] W.M. Ashraf, G.M. Uddin, M. Farooq, F. Riaz, H.A. Ahmad, A.H. Kamal, S. Anwar, A.M. El-Sherbeeny, M.H. Khan, N. Hafeez, Construction of operational data-driven power curve of a generator by industry 4.0 data analytics, Energies, 14 (2021) 1227.
[47] W. Muhammad Ashraf, G. Moeen Uddin, A. Hassan Kamal, M. Haider Khan, A.A. Khan, H. Afroze Ahmad, F. Ahmed, N. Hafeez, R. Muhammad Zawar Sami, S. Muhammad Arafat, Optimization of a 660 MWe supercritical power plant performance—a case of Industry 4.0 in the data-driven operational management. Part 2. Power generation, Energies, 13 (2020) 5619.
[48] S. Maddipati, R. Nandigam, S. Kim, V. Venkatasubramanian, Learning patterns in combinatorial protein libraries by Support Vector Machines, Computers & Chemical Engineering, 35 (2011) 1143-1151.
[49] W.M. Ashraf, G.M. Uddin, R. Tariq, A. Ahmed, M. Farhan, M.A. Nazeer, R.U. Hassan, A. Naeem, H. Jamil, J. Krzywanski, M. Sosnowski, V. Dua, Artificial Intelligence Modeling-

Based Optimization of an Industrial-Scale Steam Turbine for Moving toward Net-Zero in the Energy Sector, ACS Omega, (2023).
[50] W.M. Ashraf, G.M. Uddin, S.M. Arafat, J. Krzywanski, W. Xiaonan, Strategic-level performance enhancement of a 660 MWe supercritical power plant and emissions reduction by AI approach, Energy Conversion and Management, 250 (2021) 114913.
[51] M.E. Zayed, J. Zhao, W. Li, S. Sadek, A.H. Elsheikh, Chapter three - Applications of artificial neural networks in concentrating solar power systems, in: A.H. Elsheikh, M.E. Abd Elaziz (eds.) Artificial Neural Networks for Renewable Energy Systems and Real-World Applications, Academic Press, 2022, pp. 45-67.
[52] W.M. Ashraf, G.M. Uddin, H.A. Ahmad, M.A. Jamil, R. Tariq, M.W. Shahzad, V. Dua, Artificial intelligence enabled efficient power generation and emissions reduction underpinning net-zero goal from the coal-based power plants, Energy Conversion and Management, 268 (2022) 116025.
[53] W.M. Ashraf, V. Dua, Machine learning based modelling and optimization of post-combustion carbon capture process using MEA supporting carbon neutrality, Digital Chemical Engineering, 8 (2023) 100115.
[54] W.M. Ashraf, G.M. Uddin, S.M. Arafat, S. Afghan, A.H. Kamal, M. Asim, M.H. Khan, W.R. Muhammad, U. Naumann, S.G. Niazi, Optimization of a 660 MW e Supercritical Power Plant Performance—A Case of Industry 4.0 in the Data-Driven Operational Management Part 1. Thermal Efficiency, Energies, 13 (2020) 5592.
[55] O.K. Maurya, J.P. Ekka, D. Kumar, D. Dewangan, A. Singh, Experimental and numerical methods for the performance analysis of a tubular three-pass solar air heater, Energy, 283 (2023) 128640.